energies

MDPI

Article

Utility-Scale Grid-Connected Microgrid Planning Framework for Sustainable Renewable Energy Integration

Gerald A. Abantao [1], Jessa Alesna Ibañez [2], Paul Eugene Delfin Bundoc [3], Lean Lorenzo F. Blas [1], Xaviery N. Penisa [4], Eugene A. Esparcia, Jr. [4], Michael T. Castro [4], Karl Ezra Pilario [4], Adonis Emmanuel D. Tio [1], Ivan Benedict Nilo C. Cruz [1], Joey D. Ocon [4] and Carl Michael F. Odulio [1,*]

[1] Electrical and Electronics Engineering Institute, University of the Philippines Diliman, Quezon City 1101, Philippines; gerald.abantao@eee.upd.edu.ph (G.A.A.); lean.lorenzo.blas@eee.upd.edu.ph (L.L.F.B.); adonis.tio@eee.upd.edu.ph (A.E.D.T.); ivan.cruz@eee.upd.edu.ph (I.B.N.C.C.)
[2] Energy Engineering Program, National Graduate School of Engineering, University of the Philippines Diliman, Quezon City 1101, Philippines; jaibanez1@alum.up.edu.ph
[3] Department of Electrical Engineering, University of the Philippines Los Baños, Los Baños 4031, Philippines; pcbundoc@up.edu.ph
[4] Department of Chemical Engineering, College of Engineering, University of the Philippines Diliman, Quezon City 1101, Philippines; xnpenisa@up.edu.ph (X.N.P.); eaesparcia@up.edu.ph (E.A.E.J.); mtcastro1@up.edu.ph (M.T.C.); kspilario@up.edu.ph (K.E.P.); jdocon@up.edu.ph (J.D.O.)
* Correspondence: carl.odulio@eee.upd.edu.ph

Abstract: Microgrids have emerged as a crucial focus in power engineering and sustainable energy research, with utility-scale microgrids playing a significant role in both developed and developing countries like the Philippines. This study presents a comprehensive framework for utility-scale microgrid planning, emphasizing the sustainable integration of renewable energy resources to the distribution grid. The framework addresses the operational modes of grid-connected and islanded microgrids, emphasizing the seamless transition between these modes to ensure a continuous power supply. By leveraging local distributed energy resources, the microgrid aims to reduce dependence on the main transmission grid while enhancing resilience and reliability. The proposed planning framework not only eases the economic burden of constructing renewable energy sources but also aids distribution utilities in maximizing local resources to achieve sustainable energy goals. Through a detailed network analysis and modeling, the framework provides a robust foundation for optimizing the energy mix and enhancing the overall system performance. This research contributes to advancing microgrid technology as a key driver towards achieving UN Sustainable Development Goals, particularly in promoting clean and affordable energy access.

Keywords: distribution energy resources; microgrid; resilience; optimal energy mix; Philippines

Citation: Abantao, G.A.; Ibañez, J.A.; Bundoc, P.E.D.; Blas, L.L.F.; Penisa, X.N.; Esparcia, E.A., Jr.; Castro, M.T.; Pilario, K.E.; Tio, A.E.D.; Cruz, I.B.N.C.; et al. Utility-Scale Grid-Connected Microgrid Planning Framework for Sustainable Renewable Energy Integration. *Energies* **2024**, *17*, 5206. https://doi.org/10.3390/en17205206

Academic Editor: Angela Russo

Received: 16 August 2024
Revised: 20 September 2024
Accepted: 23 September 2024
Published: 19 October 2024

1. Introduction

Microgrids have been a major topic in power engineering research for more than a decade now [1] and both developed and developing countries like the Philippines have already deployed this technology in their existing grid network [2]. Some are isolated, supplying remote areas such as rural island communities, while others are utility-scale, connected to a local distribution grid. Utility-scale microgrids, in particular, operate in two modes: grid-connected operation and islanded operation [3,4]. In grid-connected microgrid operation, the microgrid, typically a distribution grid embedded with local distributed energy resources, still largely depends on the stable and firm supply from the main transmission grid. In contrast, in an island operation initiated due to a main grid event, the microgrid has to maintain its system voltage and frequency, adequately supply its demand, and meet the power quality with only the use of its network components and with

its local generating capacity [3]. A well-planned utility-scale microgrid is able to transition between operations seamlessly and provide a supply regardless of the operation mode.

Microgrid technology is seen as one driver of the UN Sustainable Development Goals (UN SDG) [5]. It can particularly have a significant impact on the SDG7 goal which has three main themes: (1) access to an affordable and reliable energy supply, (2) an increased mix of the renewable energy resources in the entire generating capacity, and (3) a reduction in losses for enhanced energy efficiency [6]. Due to the high costs of the distribution infrastructure expansion, microgrids can utilize local energy resources and, thereby, help governments in their efforts to achieve affordable rural electrification. Through the conduct of resource assessments, a potential local microgrid supply can be identified within a remote area with its abundance of renewable energy resources. Finally, with the electrical demand center of remote areas being collocated with the local generation supply, high system losses induced by long distances of distribution lines are prevented [5,7,8].

Technical failures, economic challenges, social acceptance, and policy barriers are significant obstacles to microgrid success [9]. Many renewable energy microgrids fail within a few years due to unresolved technical issues during planning and implementation. The high initial investment and ongoing maintenance costs pose challenges to the economic viability of microgrid projects, particularly in remote areas. Moreover, community involvement is often lacking, which is crucial for the long-term sustainability of these systems. Finally, the absence of supportive policies and regulatory frameworks creates additional hurdles, making it difficult to navigate legal and bureaucratic processes necessary for microgrid development.

It is important to note that every microgrid system is unique, varying from other microgrids in terms of network size, demand size, energy resources, technologies used, and social motivations [10,11]. Hence, it is of great significance to thoroughly plan, in accordance to its specific needs, the implementation of such projects in order to maximize its benefits. Microgrid planning still remains a challenging task. A portion of existing microgrid planning frameworks were generation-based planning where these have looked into the optimization of the generator size [12–14], local energy resource allocation [15,16], and generating capacity mix [17–20], which have been the priority. Other frameworks, on the other hand, have focused on the network aspects of microgrids where the resilience [21], reliability [22], and stability [23,24] of the network before and after microgrid operation implementation were evaluated. Unfortunately, more efforts are yet to be undertaken to take into account both the generation and network planning frameworks; this is paramount as biased planning objectives may occur and cause unforeseen problems during actual operation.

As such, this work proposes a microgrid generation and network planning methodology that focuses not only on the local resource potential but also on the needed network upgrades to ensure the seamless integration of microgrid operation. Focusing on utility-scale distribution grid-connected microgrids, the proposed framework will allow distribution utilities to maximize local resources in meeting their demand and provide an uninterrupted power supply should the distribution grid become disconnected from the main transmission grid. Moreover, network components that are of concern and potential network upgrades can be identified to improve the quality of service of the distribution utilities, particularly electric cooperatives, by enabling their systems to operate in regulatory performance when operating not only as a grid-connected microgrid but also as a stand-alone islanded microgrid during natural emergencies and main grid events. Consequently, the proposed microgrid planning framework is ensured to be not only environmentally responsible but also technologically sound and forward-thinking for a sustainable energy future.

The proposed microgrid planning framework is discussed further in Section 2; the proposed framework is composed of three main steps, namely, the identification of planning objectives, generation planning, and network planning. In Section 3, the proposed planning framework is applied to the distribution network of an electric cooperative in Kalinga, Philippines as a case study. Further, in this section, the implementation of the proposed

planning framework on this specific area was detailed and the resulting findings and recommendations were highlighted. Lastly, Section 4 concludes the paper and identifies opportunities for future research.

2. Utility-Scale Grid-Connected Microgrid Planning Framework

Figure 1 summarizes the overall planning framework. The initial step is to identify the planning objectives (Section 2.1), followed by generation planning (Section 2.2) and network planning (Section 2.3). Section 3 showcases the implementation of the planning framework presented in this work to a province in the Philippines, and Section 4 concludes this work.

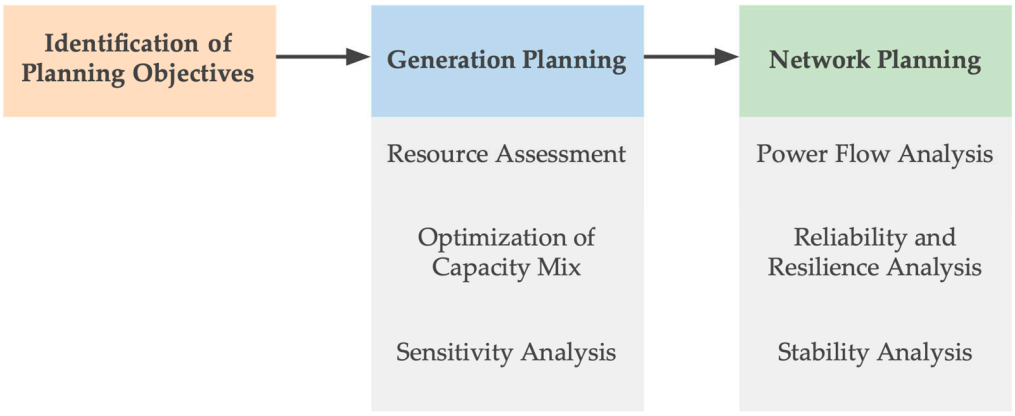

Figure 1. The overall methodology for utility-scale grid-connected microgrid planning framework.

2.1. Identification of Planning Objectives

Identifying the planning objectives is an integral part of the planning process of distribution utilities because these dictate how utility operators develop and implement their goals. Identifying the planning objectives can also minimize system losses, reduce costs due to interruption, and maximize network reliability. For the microgrid planning objectives, we mainly focus on maximizing the local distributed energy resources (DER) and maintaining the supply of critical loads, especially during contingency periods. Then, based on the identified DERs, these potential resources will be optimized to energize the whole utility-scale microgrid at various load levels. These load levels are distribution-utility-specific. Therefore, another important step in identifying the planning objectives is to identify and prioritize the critical loads in the distribution system. In this work, we defined critical loads as facilities connected to the network that are socially, economically, or operationally essential to society or community functions. The number of critical loads and their corresponding priority levels vary for every distribution utility. Hence, to identify them, it is best to use the categorizations of local agencies.

2.2. Generation Planning

Generation planning begins with assessing available local resources and then identifying the least-cost microgrid system architecture that meets local load demand. Section 2.2.1 presents the resource assessment methodologies and Section 2.2.2 presents how to determine the optimal capacity mix. To check the robustness of the identified least-cost hybrid system architecture, this work employs a sensitivity analysis as discussed in Section 2.2.3.

2.2.1. Resource Assessment

The resource assessment was conducted using geospatial data to measure the energy potential and identify suitable sites for energy utilization. This work also considered the following constraints: the ancestral domain, protected areas, tree covers, and main roads. In this work, we only considered solar, wind, and hydro resources, and the succeeding figures (Figures 2–4) show the workflow for each resource assessment. The resource assessment

methodologies presented in this paper were derived using QGIS 3.28, open-source software that supports viewing, manipulating, and analyzing geospatial data [25].

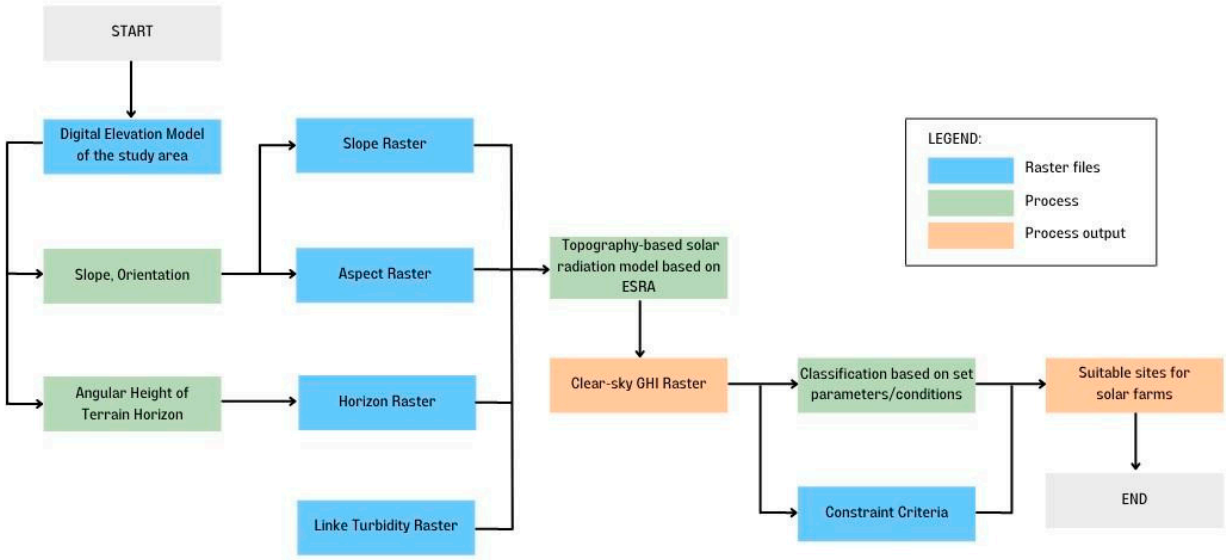

Figure 2. Workflow for the solar energy resource assessment using geospatial data.

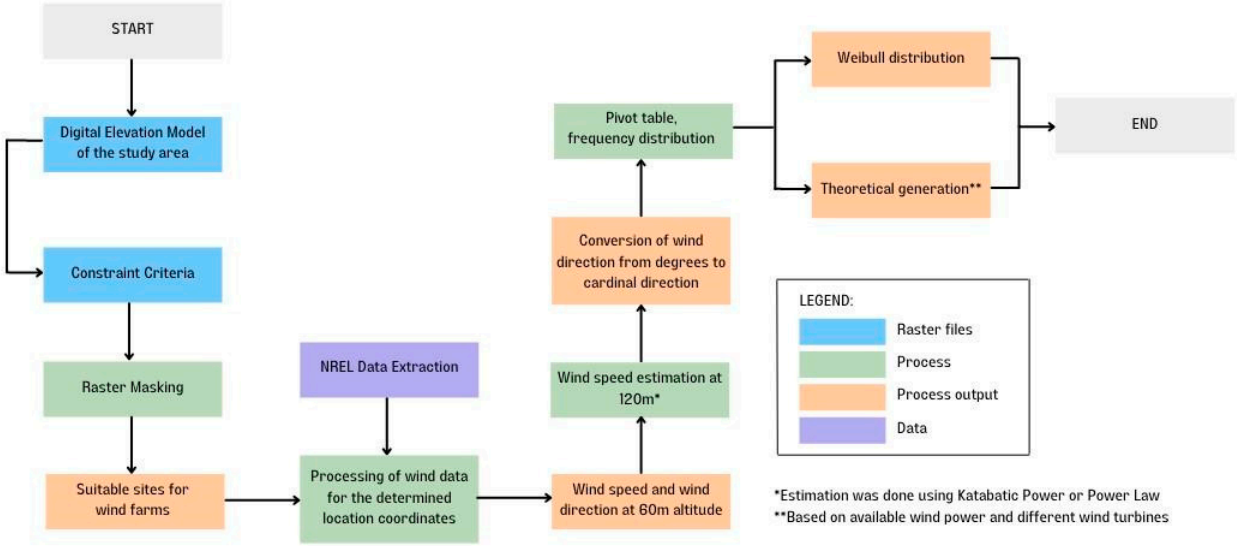

Figure 3. Workflow for the wind energy resource assessment using geospatial data.

Figure 2 shows how to compute the theoretical extractable solar energy from suitable sites for solar farms. Using the digital elevation model (DEM) of the study area, the slope and raster files are obtained through the r.slope.aspect function. The horizon raster describes the shading effect due to the sun's relative position. The Linke Turbidity raster approximates the atmospheric absorption and scattering of the solar radiation under clear skies. The four raster files (aspect, slope, horizon, and Linke Turbidity) were used as inputs to the r.sun functions, which yielded a clear-sky GHI raster. The r.sun function is a topography-based solar radiation model based on the European Solar Radiation Atlas (ESRA) model [26]. The GHI raster files were further processed based on the constraint criteria for the solar resource: ancestral domain areas, protected areas, and tree covers. Due to technical limitations, this work reduced the number of simulations, from 365 to 12 runs, based on the Julian day and incidence angle declination [27]. The monthly solar peak solar power was also obtained by considering the solar noon with the assumption

of a clear-sky setting. Solar noon is when the sun reaches its highest position in the sky at a location where the sun provides the most solar radiation. In this work, we identified the solar noon data based on the methods from NOAA Global Monitoring Division [28]. Then, we classified the clear-sky GHI raster based on the following constraint criteria—the ancestral domain, protected areas, and tree cover—to identify suitable sites for solar farms.

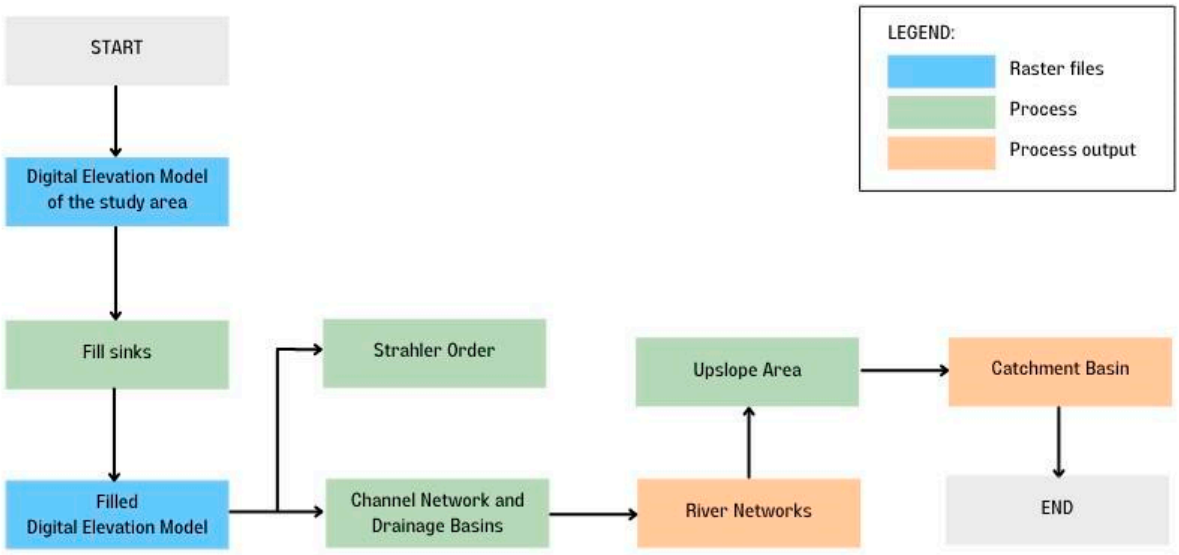

Figure 4. Workflow for the hydro energy resource assessment using geospatial data.

Figure 3 shows how the wind theoretical farm location generation is obtained and the suitable wind farm locations identified using the digital elevation models (DEMs) as the primary source of data. The constraint criteria for the wind resource are as follows: ancestral domain areas and protected areas [29]; tree covers [30]; and main roads (to ease construction) [31]. After identifying the constraints, the DEMs were masked to identify the suitable sites for wind farm installation. Wind data obtained from [32] and measured at a 60 m elevation were used to determine the coordinates of potential sites. The Katabatic power in Equation (1) was used to match the wind turbine hub height and existing wind farms with similar topographic characteristics:

$$v_2 = v_1 \times \left(\frac{z_2}{z_1}\right)^{\alpha} \tag{1}$$

where v_1 is the velocity at height z_1, v_2 is the velocity at height z_2, z_1 is the lower height, z_2 is the upper height, and α is the wind shear exponent. The wind shear exponent used is 0.4 [33], which is based on the topography of Kalinga and Apayao: having villages, small towns, agricultural land, forests, and very rough and uneven terrain. The total available energy from wind is calculated using Equation (2):

$$P_{wind} = 0.5\rho AV^3 \tag{2}$$

where ρ is the air density at 1.2 $\frac{\text{kg}}{\text{m}^3}$, A is rotor swept area in m^2, and V is the wind velocity in $\frac{\text{m}}{\text{s}}$.

The power generation of the wind turbine is determined using the Weibull distribution probability. The *shape* and *scale* factor are calculated using Equations (3) and (4), respectively:

$$shape = \left(1.2785 \times \frac{SD}{Mean}\right) - 0.5004 \tag{3}$$

$$scale = \frac{Mean}{Gamma\left(\frac{1}{1+shape}\right)} \quad (4)$$

where SD is the standard deviation of the wind speed data, the $Mean$ is the average wind speed, and $Gamma$ is the MS Excel function of the Weibull distribution probability.

The turbine power is then calculated using Equation (5) [34]:

$$P_{turbine} = \sum f(v) \times P(v) \quad (5)$$

where $f(v)$ is the probability at which a certain wind speed would occur, and $P(v)$ is the resulting power at a specific wind speed based on the turbine's power curve measured in kW.

In estimating the theoretical wind energy production, we calculated the average wind turbine periodic energy production and multiplied it by the number of wind turbines that were assumed to fill a specific location. Our assumption was based on a rule of thumb which states that the wind turbine spacing is equal to seven times the rotor diameter [35].

Figure 4 shows how the outflow points of the hydro resources are identified. We used the digital elevation models (DEMs) through the SAGA function in QGIS to identify the river networks and catch basins in the KAELCO franchise area. We also identified the watershed outflow points using the flow direction, Strahler order, and contour. Then, based on the following constraint criteria—ancestral domain areas and protected areas [29]—we excluded the outflow points that fall under these areas. Then, we used Equation (6) to estimate the flow rate in terms of precipitation and temperature [36]:

$$Q = -7.95 - 8.81 \times 10^{-4} R + 0.45T \quad (6)$$

where Q is the modeled flow rate measured in $\frac{m^3}{s}$, R is the amount of rainfall or precipitation in millimeters, and T is the temperature in °C.

2.2.2. Optimization of Capacity Mix

The next part of the DER planning process is identifying the design constraints and requirements and technical and economic modeling; hence, we assessed the optimal hybrid system architecture based on the levelized cost of energy (LCOE) using the following: the distribution utility load profile, resource data obtained from the resource assessment, and techno-economic assumptions based from the literature [37–39]. Table 1 shows a summary of the techno-economic assumptions considered in the study and Figure 5 shows the overall methodology we used to identify the optimal hybrid architecture for the microgrid system.

Table 1. Techno-economic parameters that are used in microgrid models for additional capacities.

Component	Parameter	Value	Reference
Project	Discount rate	8.28%	[38]
	Inflation rate	4.00%	[38]
	Lifetime	20 years	
	System fixed capital cost	20,000 USD	[37,39]
Solar PV Panel	Capital cost	1500 USD/kW_p	[38]
	Replacement cost	1500 USD/kW_p	
	O&M cost	15 USD/kW_p-y	[38]
	Derating factor	80%	[39]
	Lifetime	20 years	
Wind Turbine	Capacity	1.5 MW	
	Capital cost	2500 USD/kW	[38]
	Replacement cost	2500 USD/kW	
	O&M cost	25 USD/kW-y	[38]
	Hub height	120 m	
	Lifetime	20 years	

Table 1. *Cont.*

Component	Parameter	Value	Reference
Hydro Turbine	Capital cost	2830 USD/kW	[38]
	Replacement cost	2830 USD/kW	
	O&M cost	84.95 USD/kW-y	[38]
	Pipe head loss	15%	
	Available head	35.4 m	
	Efficiency	81%	
	Lifetime	25 years	
Li-ion Battery	Capital cost	800 USD/kWh	[37,39]
	Replacement cost	800 USD/kWh	[37,39]
	O&M cost	7.25 USD/kWh-y	[37,39]
	C-rate	1 kW/kWh	[37,39]
	Minimum state of charge (SOC)	20%	[37,39]
	Lifetime	10 years	
Long-duration Flywheel	Capital cost	2600 USD/kW	
	Replacement cost	2600 USD/kW	
	O&M cost	26 USD/kW-y	
	Capacity	8 kW, 32 kWh	[40]
	Lifetime	20 years	
Diesel Generator	Capital cost	600 USD/kW	
	Replacement cost	600 USD/kW	[37,39]
	O&M cost	0.03 USD/kWh	[37,39]
	Fuel cost	0.90 USD/L	[37,39]
	Lifetime	15,000 h	

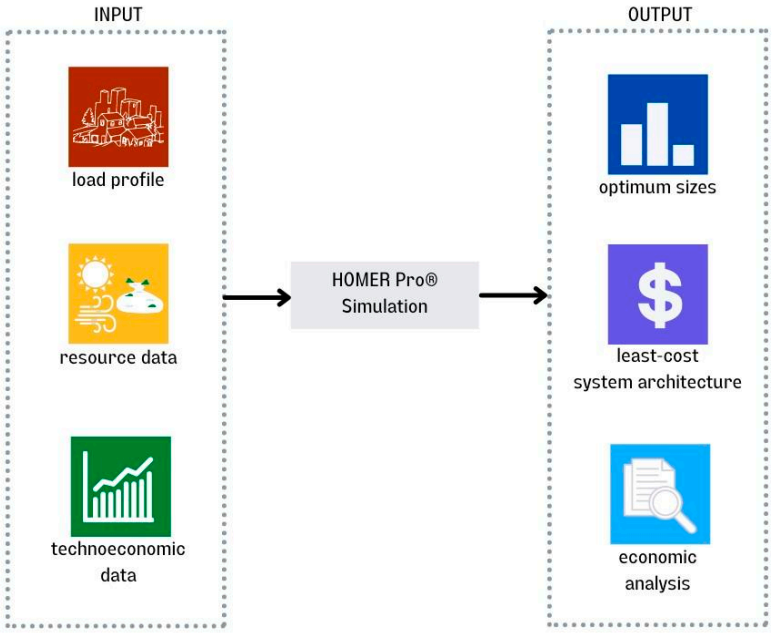

Figure 5. The overall methodology for cost-optimal hybrid system architecture.

This work considered the following energy components for the proposed hybrid energy system shown in Figure 6: solar PV, wind turbine, hydro, diesel generator, and energy storage (Li-ion battery and long-duration flywheel).

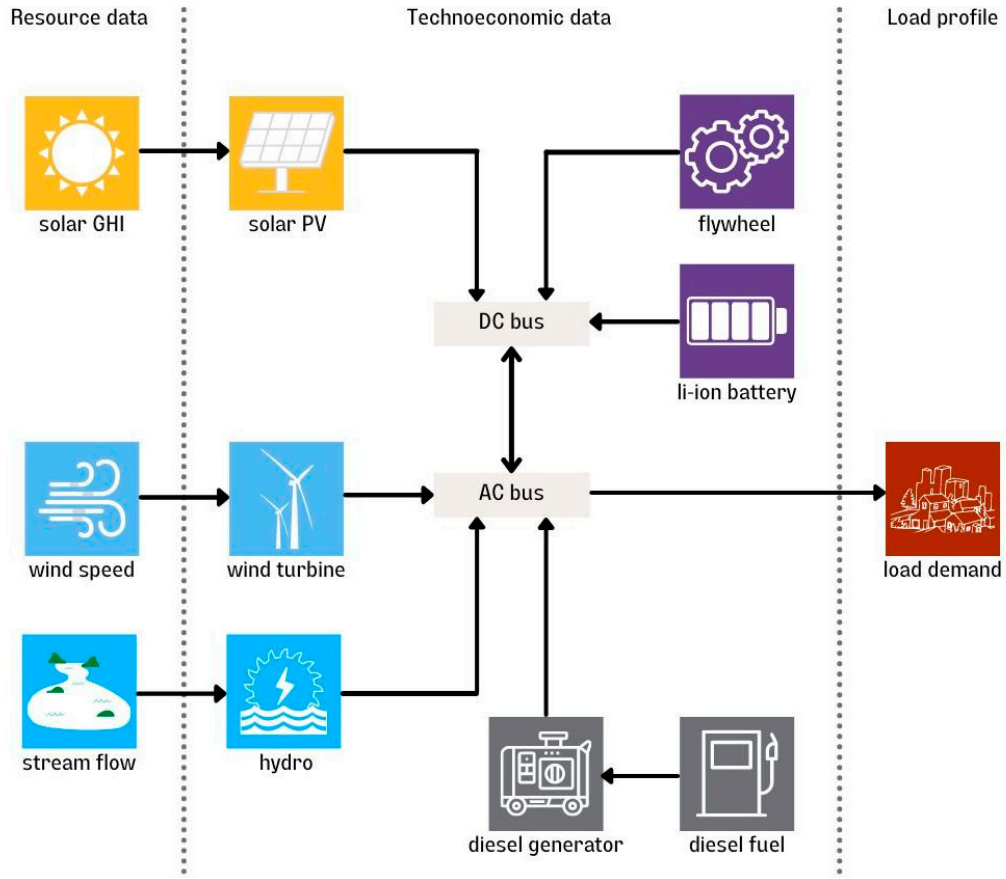

Figure 6. Hybrid system architecture for the proposed microgrid system.

The cost-optimal system architecture is identified in terms of the levelized cost of energy (*LCOE*), defined as the average cost per energy produced by the system [41]. Using the resource data, techno-economic data, and load profile, we utilized HOMER Pro® 3.14.5 to calculate additional power generator capacities and energy storage system capacities for the distribution utility. The cost-optimal system architecture was identified based on the cases and scenarios specified during the identification of planning objectives. The LCOE [41] is obtained through Equations (7)–(9):

$$NPC = \sum_{t=0}^{n} \frac{c_t}{(1+d)^t} \tag{7}$$

$$E_{served} = E_{load} + E_{grid} \tag{8}$$

$$LCOE = \frac{d(1+d)^n}{(1+d)^n - 1} \times \frac{NPC}{E_{served}} \tag{9}$$

where NPC is the present value of all future cash flows generated by the project, c_t is the net cash flow for a single period, d is the discount rate, n is the project lifetime, E_{served} is the annual energy served, E_{load} is the energy served to the load, and E_{grid} is the energy sold to the grid.

To enhance the calculation and analysis, the multi-year module from HOMER Pro® is also used, using the optimal capacity mix obtained from the single simulations. The module accounts for the component degradation, price fluctuations, non-constant increase in demand load, and system fixed O&M costs that are only extrapolated by the single simulations over the project lifetime [42]. Table 2 shows the assumptions used for the multi-year analysis.

Table 2. Assumptions used for the multi-year analysis.

	Yearly Increase	References
Grid price	2%	[43]
Fixed O&M cost	4%	[38]
Solar PV degradation	1%	[44]
Hydro (new) degradation	0	
Diesel fuel price	3.5	[45]
Load demand	yearly multiplier	[46]

2.2.3. Sensitivity Analysis

To check the robustness of the identified least-cost hybrid system architecture, we conducted a sensitivity analysis on how the changes in the load demand, fuel costs, component costs, and grid reliability affect them [39]. This was done by changing the variables one at a time, with linked variables assumed to change simultaneously. Dealing with the uncertainty of the parameters helps us see different facets of the system that may or may not be applicable in actual circumstances. The sensitivity values of each variable were obtained using the following assumptions:

Demand: +25%, +50%, +75%, and +100% of the base value;

Diesel fuel cost: −50%, −25%, +25%, +50%, +100%, and +200% of the base value;

Component costs: −50%, −25%, +25%, +50%, and +100% of the base value;

Grid reliability: 0, +25%, +50%, +75%, and +100% of the base value.

The LCOE computations are calculated under a multi-year analysis in Homer Pro® with a 20-year project lifetime. Table 3 summarizes the parameters considered in the sensitivity analysis.

Table 3. Parameters and linked variables that are used in the sensitivity analyses.

Sensitivity Variable	Linked Variables	Base Values
Load demand	Load profile	Based on case scenarios
Fuel cost	Diesel fuel cost	0.90 USD/L
Solar PV costs	Capital and Replacement costs	1500 USD/kWp
	Operating costs	15 USD/kWp-y
Wind turbine costs	Capital and Replacement costs	2500 USD/kW
	Operating costs	25 USD/kW-y
Hydro costs	Capital and Replacement costs	2830 USD/kW
	Operating costs	84.95 USD/kW-y
Flywheel costs	Capital and Replacement costs	2600 USD/kW
	Operating costs	26 USD/kW-y
Diesel generator costs	Capital and Replacement costs	600 USD/kW
	Operating costs	0.03 USD/kWh
	Diesel fuel cost	0.90 USD/L
Grid reliability	Mean outage frequency (1/yr)	12.67 outages/year

2.3. Network Planning

Beyond the resource availability and potential, the distribution network of the utility must be able to take on the additional resources and utilize them with minimal disruption even during the islanded mode. Network upgrades, determined through comprehensive network planning, can be recommended as part of the microgrid integration investment. This paper suggests the following steps of the network planning framework: a power flow analysis (Section 2.3.1), reliability and resilience analysis (Section 2.3.2), and stability analysis (Section 2.3.3). Each of these analyses identifies specific network upgrades needed to suffice the needed performance of the concerned distribution network attributes.

2.3.1. Power Flow Analysis

Figure 7 shows the flowchart for the power flow analysis. Available network data [47], typically in regulatory format, were obtained from the involved distribution utility and converted to a format usable for software simulation. The required specific data in object form were collected and the power flow of the entire network was simulated. OpenDSS (Open Distribution System Simulator), a freeware designed for simulating distribution systems [48], was chosen as the power flow analysis tool in this paper as it already has built-in models for network components. On top of it, the software's engine can be run using third-party software like VisualBasic, MATLAB, Python, etc. This feature is beneficial in automating extensive data collection.

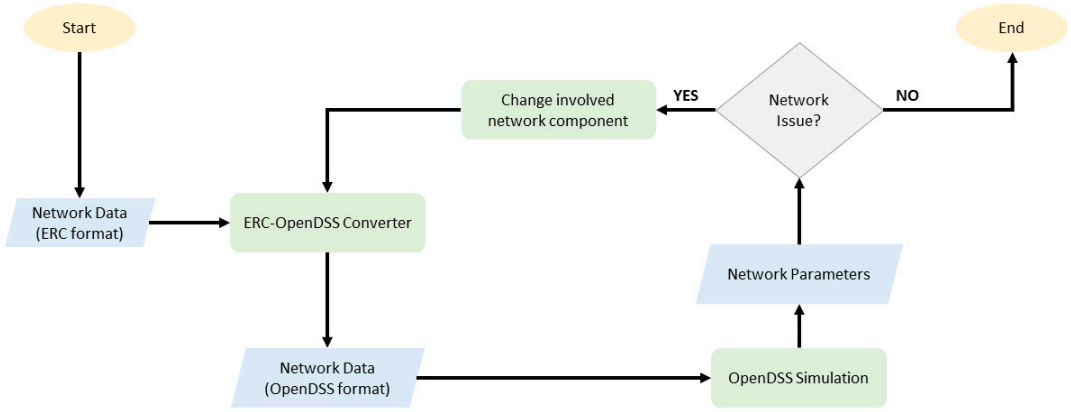

Figure 7. Power flow analysis flowchart.

After all model objects were created, the distribution network operation was then simulated. Load curve factors corresponding to the hour were multiplied by the loads' calculated peak demand to mimic the loads' daily behavior. A power flow analysis was then set to run for 24 h. Furthermore, the relevant network parameters were collected from every hour of the simulated operation for the further evaluation and characterization of the distribution network.

Based on the power flow analysis results, network components needing upgrades were identified before the conversion to a microgrid-enabled network to address existing network issues such as line overloading, transformer overloading, and undervoltage loads. Distribution lines and transformers were prioritized for upgrade, which involved uprating these components. In addressing the load undervoltage, while the transformer and line uprating could already help eliminate the undervoltage at certain loads, it was still expected that the DER integration will have a more significant effect in reducing the number of undervoltage loads.

2.3.2. Reliability and Resilience Analysis

The reliability analysis evaluates the ability of the distribution system to provide a continuous electric service to customers. This is usually in terms of the number of customer interruptions and their average duration in a certain period. In this paper, a sequential Monte Carlo (MC) reliability analysis methodology was chosen to quantify the reliability improvement brought about by a microgrid planning investment. The sequential MC involved three steps: (1) generating the artificial operating history of each network component using failure rates and mean time to repair; (2) modeling the system response to faults; and (3) calculating the reliability indices, which are the System Average Interruption Frequency Index (SAIFI) and the System Average Interruption Duration Index (SAIDI).

The corresponding reliability levels, characterized by the indices, were determined for each of the following configurations: (1) the base network and (2) the microgrid-enabled network. The microgrid-enabled network configuration uses the resulting identified DERs in the generation planning. Moreover, to enable microgrid islanding as a restoration

strategy, new switches were installed in the microgrid-enabled network configuration as an additional network upgrade; the methodology used to identify the placement of new switches is discussed in the latter part of this section.

As distribution system resilience is more concerned with widespread and long-term outages, assessing it is quite different from determining reliability. Hence, in contrast to the reliability analysis methodology, the nonsequential Monte Carlo simulation, initially proposed in [49], was chosen to analyze the level of resilience before and after the microgrid investment. In this simulation, the analysis is on a per-scenario basis wherein the distribution network—the same network configurations from the reliability analysis—is subjected to extreme events with randomness introduced to their specific parameters. The three steps of the nonsequential MC simulation are, namely, the extreme event modeling, the damage assessment, and the calculation of resilience metrics.

The typhoon was the extreme event considered in the case study as it is the most common in the Philippines. This extreme event is typically modeled using the probability distribution of its maximum sustained wind speed. The Gumbel probability distribution is suggested for this modeling as it can effectively characterize extreme wind speeds. The impact of the typhoon extreme event on the distribution system was modeled through the use of component fragility curves which show the wind-speed-dependent failure probability of each component. Such curves are typically generated from a wide range of historical data. However, when such data are difficult to obtain, empirical failure equations can also be used instead; Equations (10) and (11) [49] model the fragility of the distribution poles and overhead lines, respectively:

$$FP_{pl} = 0.0001 \times e^{(0.0421 \times V_w)} \tag{10}$$

$$FP_{ij} = 1 - \prod_{pl=1}^{NP} \left(1 - FP_{pl}\right) \tag{11}$$

$$\gamma_{ij}^{line} = \begin{cases} 1, & if\ FP_{ij} \geq x_{line} (= \cup(0,1)) \\ 0, & otherwise \end{cases} \tag{12}$$

$$MTTR = \begin{cases} MTTR_{normal}, & v_{max} \leq 20\ \mathrm{m/s} \\ a_1 \times MTTR_{normal}, & 20\ \mathrm{m/s} < v_{max} \leq 40\ \mathrm{m/s} \\ a_2 \times MTTR_{normal}, & 40\ \mathrm{m/s} < v_{max} \leq 60\ \mathrm{m/s} \end{cases} \tag{13}$$

$$where:\ a_1 \sim \cup(2,4)\ and\ a_2 \sim \cup(5,7)$$

where FP_{pl} is the failure probability of the distribution poles, FP_{ij} is the failure probability of the line section between bus i and j, V_w is the maximum sustained wind speed value during the extreme event measured in $\frac{\mathrm{m}}{\mathrm{s}}$, NP is the number of poles between bus i and j, γ_{ij}^{line} is the failure status of a component, $MTTR$ is the mean time to repair of the component in h, and v_{max} is the maximum sustained wind speed value during the extreme event in $\frac{\mathrm{m}}{\mathrm{s}}$.

Damage assessment was carried out each time a typhoon extreme event scenario was generated. It starts by determining the failure status of the components by comparing each failure probability with a uniformly generated random number [49]. The repair process starts once all the information regarding the faulted components has been gathered. In this project, the effect of the extreme event on the mean time to repair of each component is considered using a multiplier for every level of intensity, which is based on the maximum wind speed [50]. The fault isolation system restoration strategy in the reliability analysis was also used in this methodology.

The resilience metrics used in this planning framework are based on [51] which focus on the ability of the system to maintain the supply of power to the critical facilities during extreme events; critical facilities are loads from sectors that are crucial in the functioning of the community, especially during emergencies. The standard reliability indices (SAIFI, SAIDI, and EENS) were reconceptualized to count interruptions experienced

by loads grouped into priority levels. Depending on the current needs and concerns of the distribution utility, e.g., the utility may currently give emphasis to emergency-response loads over residential loads, the weights for the set of resilience metrics for every priority level can be assigned accordingly. The formulation of the SAIFI resilience metric is described in the equation below; the SAIDI and EENS resilience metrics were formulated in the same manner:

$$SAIFI^{event}_{priority(l)} = \frac{\sum N^{int,LP}_{priority(l)}}{N^{T}_{priority(l)}} \tag{14}$$

$$SAIFI^{event} = \sum_{priority\ levels} \left(w_{priority(l)} \times SAIFI^{event}_{priority(l)} \right) \tag{15}$$

where $SAIFI^{event}_{priority(l)}$ is the average system interruption frequency index considering customers with priority level l for a particular extreme event measured in customer-interruption/event, $SAIFI^{event}$ is the composite system interruption frequency index of the system during a specific extreme event measured in customer-interruption/event, $N^{int,LP}_{priority(l)}$ is the number of interrupted customers with a priority level (l), $N^{T}_{priority(l)}$ is the total number of customers with priority level l in the system, and $w_{priority(l)}$ is the weight assigned to a priority level, which may vary according to the utility's concerns.

To maximize the benefits of the microgrid investments, specifically the integration of DERs, network upgrades in the form of additional switches are needed. The installation of new switches will be of great help in optimizing the distribution network's reliability and resilience performance as it allows the formation of microgrid islands, supported locally by DERs, whenever an interruption occurs. This will ensure the continuous energization of loads and, most importantly, critical loads. Consequently, the minimization of interruptions was chosen to be the objective of the optimization of these network upgrades. To aid this, the data from the results of the resource planning were used to identify the connection points of the dispatchable DERs.

To reduce the computational burden, network upgrade optimization considers only the primary MV network, including the primary overhead lines, switches, and distribution transformers. Hence, the secondary overhead lines and service drops were removed, and the loads were connected directly to their corresponding distribution transformers. Another preliminary step was to select the candidate sections where the new switches would be optimally allocated. The selection is meant to impose a load prioritization scheme, which is a part of resilience, such that an installed switch will disconnect as few critical loads as possible. Moreover, this set of candidate sections excludes lateral feeder sections and, hence, includes the main feeder sections only.

Using the Greedy Randomized Adaptive Search Procedure (GRASP) method proposed in [52], the allocation of the new switches was optimized with the objective function considering two opposing functions: (1) the cost of an improvement in reliability, expressed in expected energy not served, and (2) the total cost of installing switches. The flowchart of this metaheuristic method and the definition of the objective function are shown in Figure 8.

The objective function is as follows:

$$min\ f = c_{switch} \times n_{switch} + c_{EENS} \times EENS_{swall} \tag{16}$$

where c_{switch} is the cost associated with installing a single switch in USD/switch, n_{switch} is the number of allocated switches, c_{EENS} is the cost associated with expected energy not served in USD/MWh, and $EENS_{swall}$ is the expected unserved energy when the switch allocation is *swall* in MWh.

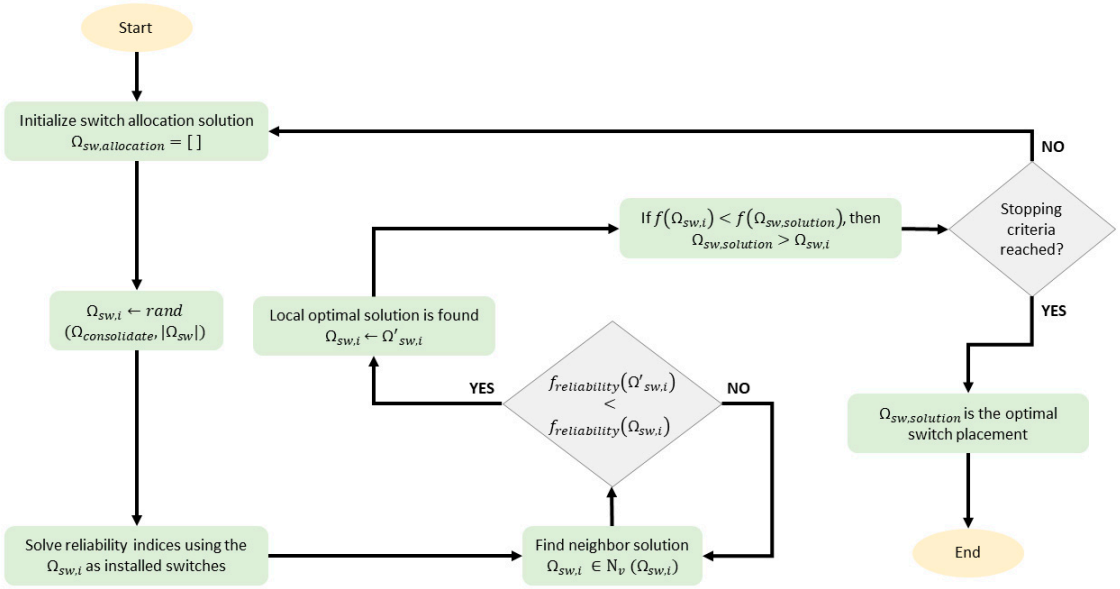

Figure 8. Optimal switch allocation flowchart.

A set of switch allocations is randomly selected from the group of candidate feeder sections at each iteration. Using this set of switch allocations, the reliability of the distribution network is evaluated analytically, and, afterwards, the objective function is computed. It is to be noted that the DERs allowed to form islands and restore power after a fault are only the dispatchable ones (hydro and diesel). The next step in GRASP, also known as the local search step, is to investigate the neighbor solutions of the current iteration's switch allocation—a neighbor solution is a set of switch allocations wherein one switch is reallocated to the other edge of its corresponding branch [52]. The neighbor solutions are evaluated one by one, and the first neighbor solution to improve the objective function replaces the current iteration's switch allocation. Finally, if the objective function of the existing switch allocation is lesser than the incumbent best switch allocation solution, then the current switch allocation becomes the incumbent best solution. This process is repeated until the maximum iteration is reached.

2.3.3. Stability Analysis

The frequency stability of the distribution network can be a matter of concern when DERs are integrated and microgrid operation is enabled. Maintaining a power supply with a stable frequency and voltage requires that there is sufficient power generation available to supply the demand [53]. This issue is rarely encountered in distribution planning as the stability responsibility is typically relegated to the transmission operators. Nevertheless, independence from the larger grid prompts the need for self-monitoring and regulation. When unregulated, the frequency or voltage may fluctuate heavily and can spiral out of control during events such as grid disconnection, load dropping, or loss of supply. When transients occur, the system should be able to adjust to changing demand and shift to a stable operating condition without crossing any regulatory power quality constraints.

In this paper, the microgrid stability analysis focuses on the frequency stability of the distribution network during grid disconnection events, operating locally as a single microgrid island. The independent microgrid should provide sufficient power to the local loads while satisfying the same power quality constraints as during the grid-connected mode. The local generation should be able to gracefully transition from any mode, whether it is serving the local demand or exporting excess generation into the grid, into an islanded mode where generators can either supply the microgrid demand's various requirements and shift while satisfying the same power quality constraints as during the grid-connected mode. The local generation should be able to transition from any mode smoothly, whether it

is serving the local demand or exporting excess generation into the grid, or into an islanded mode where generators can either supply the microgrid demand's various requirements and shift needs or standby into a reserve function that can act upon the requirements of critical loads

The goals of the stability simulations are to simulate the interactions between the microgrid's proposed DERs and see if the network can gracefully transition from a grid-connected state into an independent microgrid without critical issues in power quality. All stability simulations are set up and run using MATLAB Simulink 2021b.

The simulated microgrid is modeled as a single bus network to simulate the DER interactions while reducing the expected complexity of a distribution network. While actual distribution networks are vast and expansive, a reduced network simulation will still provide the necessary information, mainly because the proposed generation in this network is centralized towards the primary network. This setup minimizes the calculation time and complexity while still establishing stability limits based on the capabilities of the proposed generation. However, this approach does ignore the effects of the network line strength and line capacities, and all power flows are assumed to be lossless.

All proposed generation sources—solar PV, wind turbine, hydropower, battery storage, and diesel—are represented by Simulink models. The sizes of the DERs in the simulated network follow the resource assessment recommendations. As for the generator models, the solar power generator is represented by Simulink solar panel models optimized by MPPT and converted using the average functions of DC–DC and DC–AC converters. Synchronous generator-based wind turbine models represent wind power generation. Hydro-power and diesel generation use synchronous generation. Finally, the battery model is assumed to be completely discharged and not drawing power as a corner case. Figure 9 illustrates the model's blocks, including generation sizes recommended from the resource assessment.

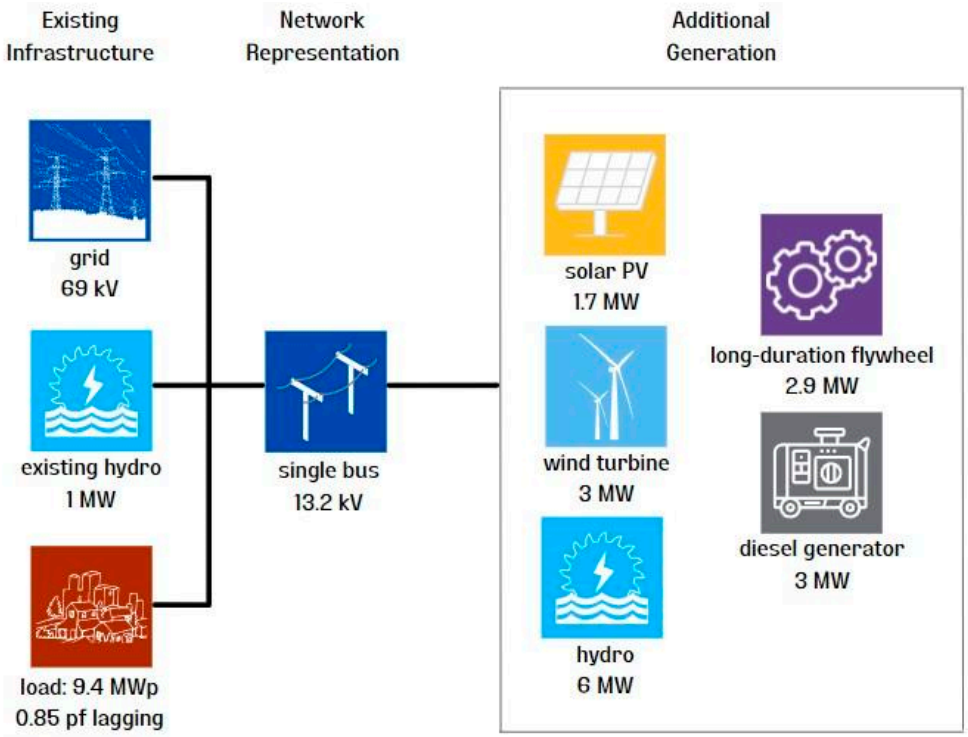

Figure 9. Single bus network model.

A single apparent power load represents the load. The power factor is maintained at 0.85 lagging, and the base demand is set at 9.4 MW based on utility consumption data. The system loss of the complete system is assumed to be a component of this base demand.

To assess the frequency stability of the single bus network, islanding scenarios are run with a constant base demand and varying amounts of non-dispatchable power. The stability is maintained by the inertia of the connected synchronous generators (diesel and hydroelectric plants). The irradiance and wind speed inputs to the solar and wind plants are adjusted to simulate varying amounts of active power flowing through or from the grid before the grid disconnection or islanding event. For all test cases, an islanding event is initiated after achieving a steady-state operation and run to see if the stability is maintained. The last test case introduces a frequency protection relay to disconnect the non-dispatchable generation when the frequency crosses a magnitude limit to respond to the changes in frequency during islanding. For frequency stability scenarios, the non-dispatchable solar and wind generation varies by changing the input irradiance and the number of wind turbines, as illustrated in Table 4. Two additional scenarios using frequency relays use test scenario 1, with relays set to disconnect the solar and wind generation upon encountering 62.4 Hz and 61.86 Hz, respectively.

Table 4. Stability test scenarios made by changing variable generation and demand [54].

Test Scenario	Irradiance (W/m^2)	Wind Turbines	Real Power Demand	Pre-Islanding Grid State
1	1000	2	9.4 MW	1.70 MW exported to grid
2	1000	4	9.4 MW	4.70 MW exported to grid
3	250	2	9.4 MW	0.13 MW imported from grid
4	0	0	9.4 MW	1.10 MW imported from grid

The stability of the frequency is based on the magnitude and duration of deviations from the nominal frequency of 60 Hz. Any deviations and restoration behaviors are compared against the Philippine grid codes for stable frequency and mandatory generator disconnection. The regulatory restrictions are listed in Table 5. When the frequency experiences an increase of 4%, the regulation requires that any DERs immediately disconnect to prevent damage.

Table 5. Allowable operating durations for ranges of frequency deviation in embedded generating plants [55].

Frequency		Operating Duration
Hz	**p.u.**	
>62.4	>1.04	Automatic disconnection
61.8–62.4	1.03–1.04	5 min
58.2–61.8	0.97–1.03	Continuous operation
57.6–58.2	0.96–0.97	5 min
<57.6	<0.96	5 s

From the results of the stability analysis, additional control and protection upgrades can be recommended. The inertia from the additional synchronous generator (diesel) is hypothesized to be enough to maintain the nominal frequency during islanding. Frequency relay settings can be configured to address the deviations beyond the allowable nominal frequency range, consequently, controlling the output of the non-dispatchable variable generators such as wind and PV.

3. Case Study: Kalinga Province, Philippines

This work applied the utility-scale grid-connected planning framework to a grid-connected distribution utility in the northern Philippines, the Kalinga-Apayao Electric Cooperative, Inc. (KAELCO), (Tabuk City, Kalinga, Philippines) which provides electricity to Kalinga and some municipalities of Apayao. Figure 10 shows the KAELCO franchise area and its feeder network. In 2019, residential customers of KAELCO accounted for

the majority of the energy sales at 69.48%, while commercial and industrial customers accounted for 18.20% [56]. The peak demand for this distribution utility is at 9.4 MWp. KAELCO is connected to the Philippine Luzon grid, with electricity sources within and outside its franchise area. A one-megawatt (1 MW) run-of-river hydroelectric plant located at Tabuk City, Kalinga, provides power to KAELCO, together with a coal-powered plant under a power supply agreement [56]. The remaining load demand is met through the wholesale electricity spot market (WESM) [56]. Currently, KAELCO has three main feeders and a 10 MVA substation located at Tabuk City, Kalinga, serving all the Kalinga municipalities and the Conner municipality in Apayao. Other unconnected parts of the franchise area are locally supplied by small diesel power plants and are not considered in this paper.

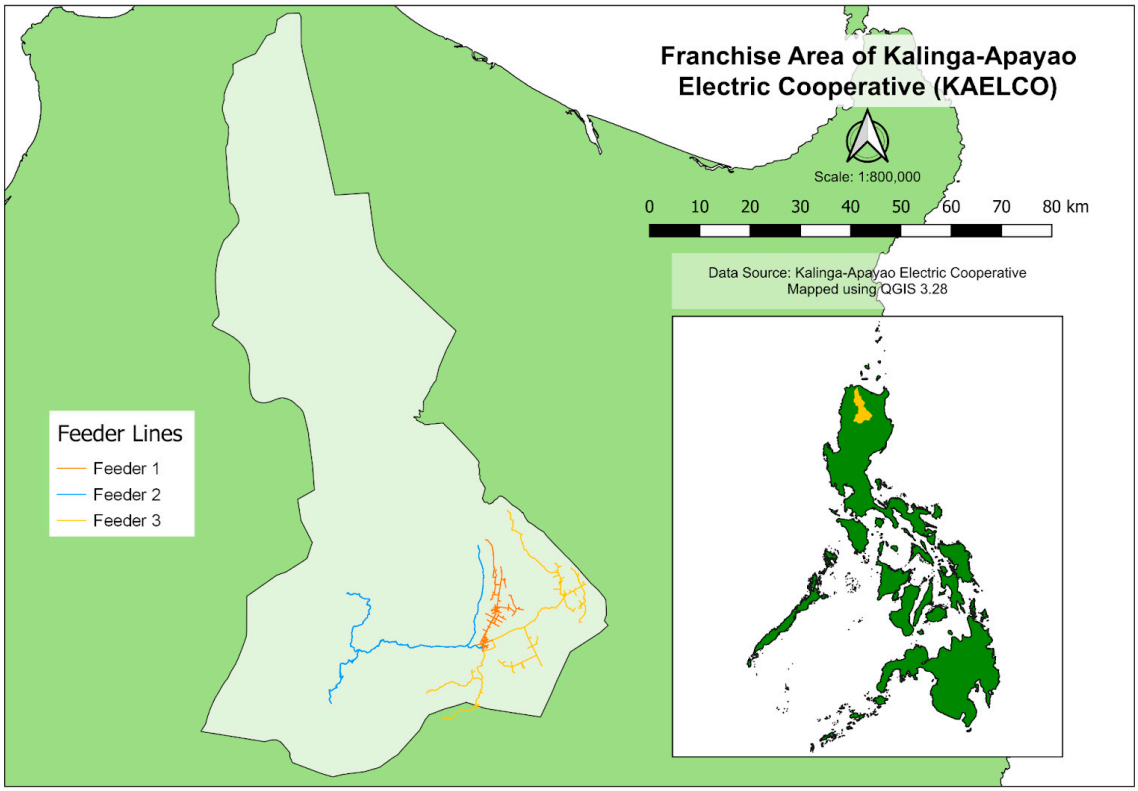

Figure 10. Franchise area of Kalinga-Apayao Electric Cooperative, Inc. (KAELCO).

The Philippine Department of Energy designated some parts of the Kalinga-Apayao area as a "competitive renewable energy zone" in a recent report prepared with the United States Agency for International Development (USAID) and the National Renewable Energy Laboratory (NREL) [38]. The report aims to direct renewable energy projects within economic locations in the Philippines [38]. In addition, the KAELCO franchise area covers a mountainous terrain and vast river network, indicating the substantial potential for the development of run-of-river power plants. However, the available regions for installing renewable energy generators are limited since most places within KAELCO are protected areas and ancestral lands, aside from the mountainous terrain. These lands have exploration and development constraints that developers must consider, following the Philippine laws [57,58].

3.1. Identification of Planning Objectives

The Critical Facility Areas classification developed in [59] was used to identify the critical loads connected to the KAELCO distribution system while the load prioritization considered in this study was based on the Risk Category of Buildings and Other Structures from the International Building Code [60] as summarized in Table 6. While Priority Levels 3 and 4 loads are considered critical loads, only Priority Level 4 loads require a continuous

power supply. The supply requirement for Priority Level 4 is mainly due to the life-threatening consequences should the distribution network fail to operate. Priority Level 3 loads are facilities that are also important during emergencies as these can serve as evacuation shelters and transport. The distribution of loads based on this prioritization is shown in Figure 11.

Table 6. Load prioritization levels that are based on risk categorization [59,60].

Level	Electrical Loads
Priority 4	Health and welfare, emergency and defense, government, energy production, water supply, communications, flood control, and waste management facilities
Priority 3	Education, cultural, major commercial, heavy industry, transportation, food security, and big leisure facilities
Priority 2	Small residential buildings, and restaurants
Priority 1	Agricultural facilities, and minor storage facilities

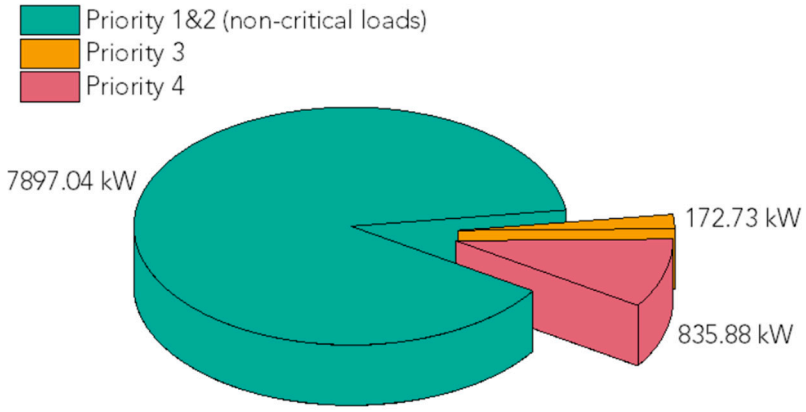

Figure 11. Peak load demand in KAELCO for each priority level.

It can be observed that only a small fraction of the load peak demand corresponds to critical loads. These were mainly from the government sector (such as local government offices and barangay halls) and the communication sector (such as telecom towers and TV and radio stations). This is expected as the majority of the customers of KAELCO are residential customers. The percentages corresponding to each priority level were used in some of the subsequent sections.

First, this work explored two scenarios:

Scenario 1: This is the base scenario (existing energy system configuration of KAELCO), where the combination of its existing one-megawatt (1 MW) mini hydroelectric power plant and the main grid supplies its total load demand;

Scenario 2: This is a modified energy system configuration with sellback. The modified energy system configuration consists of the grid-connected KAELCO utilizing its 1 MW mini hydroelectric power plant plus the additional energy resources identified in Section 3.2.2.

Then, based on the identified total and critical load demands, this work presents three (3) case studies under Scenario 2:

Case 1: The energy system configuration supplies the total KAELCO load demand (Priorities 1, 2, 3, and 4);

Case 2: The energy system configuration supplies to Priorities 3 and 4 loads only;

Case 3: The energy system configuration supplies to Priority 4 loads only.

3.2. Generation Planning

3.2.1. Resource Assessment

The renewable energy resource assessment was conducted using the LiDAR data obtained from LiPAD Team, UP Training Center for Applied Geodesy and Photogrammetry, University of the Philippines Diliman [61]. The digital elevation model (DEM) of Kalinga and Apayao was used throughout the resource assessment. Figure 12 presents the available solar (Figure 12B), wind (Figure 12C), and hydro (Figure 12D) energy resources within the KAELCO franchise area (Figure 12A).

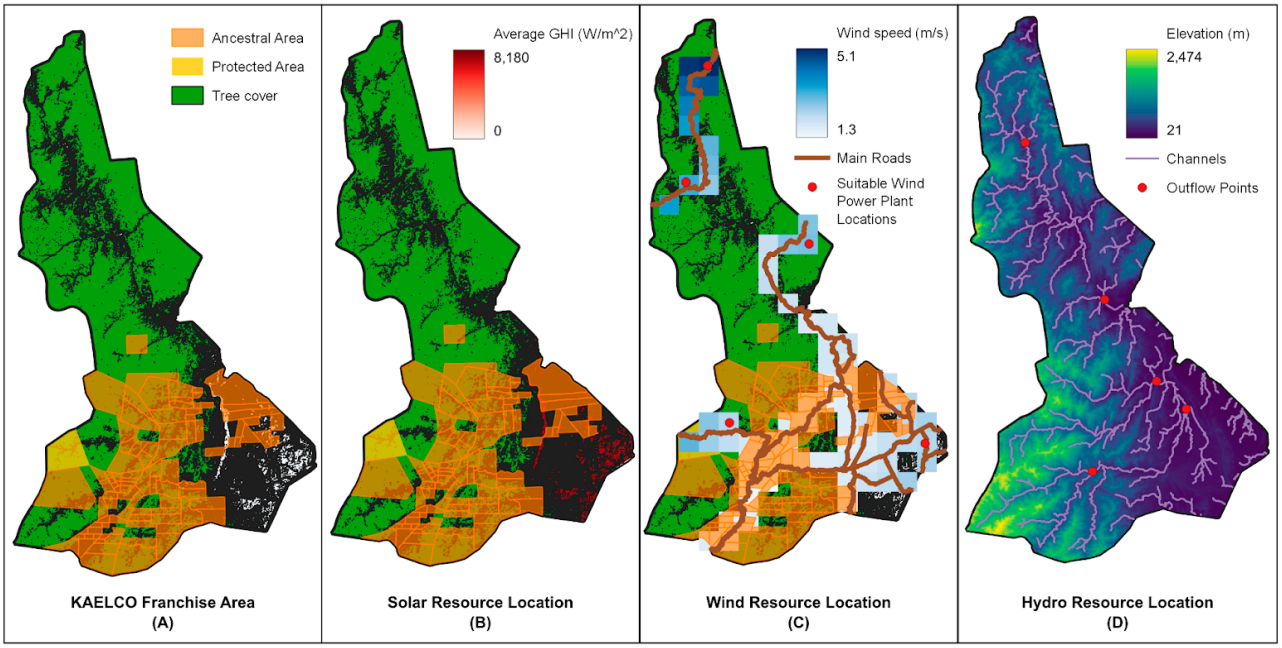

Figure 12. Locations of the available renewable energy resources within the KAELCO franchise area. Mapped using QGIS 3.28.

The results of the solar resource assessment shows that Tabuk City and the Municipality of Rizal, both located in Kalinga, are the most suitable sites for solar PV installations after excluding the ancestral domain and protected areas [29] and tree covers [30] (Figure 12A). However, it eliminated a considerable portion of the land, leaving a usable space of 805.46 km^2. Based on the average solar GHI level of 7186.09 Wh/m^2-day, the usable area is translatable to available solar energy resources of 5788.11 GWh/day or 2,114,106.47 GWh/year.

Another criterion considered for the solar resource assessment is the topographic slope of the area. Since the Kalinga and Apayao provinces are mountainous, building solar farms in these areas might lead to engineering and financial issues. The slopes identified in these provinces ranged between 0 to 89.55 degrees with a mean value of 18.85 degrees, signifying a good location since a suitable location for a solar farm should have a slope lower than 35 degrees [62]. The slopes with values from 0 to 35 were reclassified, which calculated a total available contiguous area of 3529.36 sq. km. Based on the average annual solar GHI level of the suitable area, which is equal to 7021.78 Wh/m^2-day, the available solar energy is about 24,782.43 GWh/day or 9,051,783.14 GWh/year. Meanwhile, based on the 1077.71 W/m^2 average peak power of the usable area, the total available area is translatable to 3803.63 GW of extractable solar power. The available solar energy is more than enough to supply the power demand of KAELCO.

Based on the existing wind farms with similar topographic characteristics to Kalinga and Apayao, the required hub height for the wind turbine is about 120 m. Since we used data [32] measured at a 60 m elevation, we extrapolated the wind speed at 120 m using

the Katabatic power equation. Results from the wind resource assessment identified five potential locations for wind farm installations after taking into account the ancestral domain and protected areas [29], and main roads [31] (Figure 12C). The main roads, including primary and secondary roads, were considered a criterion because these would ease the economic burden of constructing the wind farms [31]. There were three suitable locations in Apayao (two in Calanasan, and one in Kabugao), and two in Kalinga (Balbalan and Rizal). The average periodic wind turbine energy production for each location was calculated to estimate their theoretical energy production, assuming that the total available area is filled with wind turbines. A rule of thumb is that the wind turbine spacing equals seven times the rotor diameter [33]. Table 7 provides the theoretical energy production in MW for the identified five suitable locations.

Table 7. Suitable wind farm locations and their corresponding annual energy production.

Location (Centroid)	Mean Wind Turbine Periodic Energy Production (MWh)	Number of Turbines Based on 5 km Resolution	Theoretical Energy Production (MWh)
18.13, 121.02 Calanasan, Apayao	10,014.25	180	1,802,565.00
18.43, 121.07 Calanasan, Apayao	13,703.71	216	2,960,001.36
17.98, 121.33 Kabugao, Apayao	6193.07	252	1,560,653.64
17.52, 121.13 Balbalan Kalinga	17,409.28	72	1,253,468.16
17.47, 121.62 Rizal, Kalinga	10,928.51	216	2,360,558.16
		TOTAL	9,937,246.32

Based on a 5 km resolution, 936 wind turbines with a rotor diameter of 120 m can be installed within the KAELCO franchise area. This number of turbines has theoretically a total periodic energy production of 9937.25 GWh, which is more than enough to cover the KAELCO load demand at 9.4 MWp.

The hydro resource assessment identified six catchment basins, but only five were considered because the other one is too small compared to the others. Furthermore, the watershed at the bottom-most region (Figure 12D) is within the ancestral lands; thus, putting up a hydropower plant there might start political unrest. As a result, the watersheds were reduced to four, and the outflow points were determined using the flow direction, Strahler order, and contour.

The total hydroelectric energy that can be generated within the KAELCO franchise is summarized in Table 8 according to hydroelectric turbine types that might be used in the installation. The computations also assumed that the flow rate is equal for all the output points of the four identified watersheds (Calanasan, Apayao; Conner, Apayao; Pinukpuk, Kalinga; and Tabuk City, Kalinga). The assumption was based on the realization that the Strahler orders are equal across all outflow point locations and that the net head requirement could be met due to the topographical characteristics of these locations.

Table 8. Total energy generation from the four watersheds within the KAELCO franchise area using different types of hydroelectric turbines.

Turbine Type	Total Energy Generation (GWh/Turbine)
Kaplan	4.32
Crossflow	8.64
Francis	17.27

The results from the resource assessment support the technical report [38] that classified some parts of the Kalinga-Apayao area as a "competitive renewable energy zone". The resource assessment also quantified how many of these renewable energy resources can potentially be maximized for future energy projects.

3.2.2. Optimization of Capacity Mix

Figure 13 shows the KAELCO load profile used in the analysis. The hourly dataset has 8616 data points from 1 January to 25 December of 2019, with a peak load of 9404.64 kW and a peak month in June. The hourly load profile also shows peak demand between 7 and 10 in the evening.

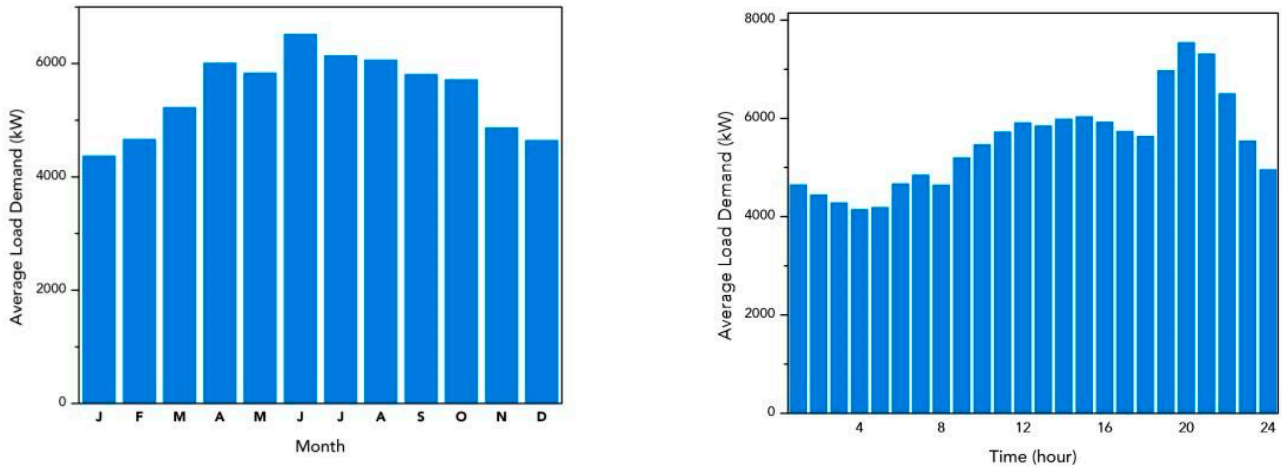

Figure 13. KAELCO monthly (**left**) and hourly (**right**) load profiles.

Table 9 summarizes the average values for solar, wind, and hydro resources obtained from the resource assessment and used in identifying the optimal capacity mix for the KAELCO franchise area.

Table 9. Average values for solar, wind, and hydro resources used.

Resource	Parameter	Value
Solar	Monthly Global Horizontal Irradiance (GHI)	3–5 kWh/m^2-d
Wind	Monthly average wind speed	4–9 m/s
Hydro	Monthly average stream flow	1000–4000 L/s

In the techno-economic costs, the capital costs for the solar PV panel, wind turbine, and hydro turbine follow the assumed exchange rate of PHP 50.6074 per USD (average, September 2019 to August 2020) from the Bangko Sentral ng Pilipinas [38]. Replacement costs are assumed to occur at the end of the component lifetime, using the inflation rate of 4.0% [38]. Inverter costs are already embedded in the solar PV panel costs. This work also identified the flywheel costs relative to what is available in the Philippine market. For the grid-connected scenarios, the study used the grid power price of 0.12 USD/kWh and the selling price of 0.08 USD/kWh based on the energy rates provided by KAELCO as of 2021.

The capital and O&M costs used for the existing 1 MW hydropower plant within the KAELCO franchise area are based on the 2013 ERC Application of the plant [63]. In converting the nominal costs (2013) to real costs (2020), the ratio of 2013 CPI (102.6) and 2020 CPI (123.30) was used as the conversion factor with the assumed exchange rate of 50.6074 PHP/USD. In the model with the base year in 2019, the hydropower plant used in the analysis has an assumed remaining lifetime of 20 years following its commercial operation in 2016.

Additional investment costs include switches and are discussed in detail in Section 3.3.2. There are also other expected costs from the short-circuit capacity and control system upgrade.

All simulations adopt a load-following dispatch strategy where a diesel generator only generates enough power to meet the demand [64]. Random outages were considered to simulate Scenario 2 (grid-connected microgrid) and reflect the grid reliability in the system. When there is a network failure, all other system components supply the load demand. The study used the mean outage frequency of 12.67 per year, mean repair time of 3.78 h, and repair time variability of 60.64%. These data were derived using the average power supply interruption in the KAELCO grid for six years. The criterion of prohibiting the grid from charging storage was also applied. For the project constraints, the operating reserve as a percentage of renewable output (solar and wind) is set to 0 since the simulations already included storage in the system.

In this work, we only considered the hybrid system configurations with the lowest generated levelized cost of energy (LCOE). Table 10 summarizes the optimal system architecture using a multi-year analysis.

Table 10. Optimal hybrid system architecture with the lowest LCOEs.

	Solar PV	Wind Turbine	New Hydro	Existing Hydro	Diesel Generator	Long-Duration Flywheel	LCOE (USD/kWh)
Scenario 1	-	-	-	1 MW	-	-	0.145
Scenario 2							
Case 1	1.7 MW_p	3 MW	6 MW	1 MW	3 MW	2.9 MW	0.114
Case 2	-	-	6.9 MW	1 MW	-	-	0.113
Case 3	-	-	6.9 MW	1 MW	-	-	0.116

Note: Scenario 1: existing energy system configuration; Scenario 2: modified energy system configuration with sellback; Case 1: microgrid system that supplies the total energy demand; Case 2: microgrid system that supplies 11.33% of the total load, corresponding to critical services; and Case 3: microgrid system that supplies to 9.39% of the total load, corresponding to critical services.

Even though we considered lithium-ion batteries and flywheels for energy storage in the analysis, only the flywheel made it to the optimal system architecture, at least for Scenario 2, Case 1. A report on microgrids with energy storage [19] details the benefits of using the flywheel as the energy storage system. The results also show that the LCOE values of KAELCO's existing energy system configuration (Scenario 1) at 0.145 USD/kWh are higher than the modified energy system configuration (Scenario 2) with LCOE values ranging from 0.113 USD/kWh to 0.116 USD/kWh.

The difference in LCOE values can be attributed to the diversified capacity mix rather than solely relying on the grid to meet its load demand, as shown in Figure 14 (left). The base scenario might be considered the least-cost system at the time. However, in the case of the Philippines which is mainly coal-powered, importing coal means that the system is inflexible and vulnerable to price instability and high prices [65]. At the same time, the abundance of renewable resources (solar, wind, and hydro) within the KAELCO franchise area allows the immediate application of the microgrid system to promote the flexibility of their grid.

In terms of operation hours shown in Figure 14 (right), hydro is the most utilized resource all year round, followed by wind at 7442 h and solar at 4335 h. Meanwhile, the diesel generator in Scenario 2, Case 2 operates at 16 h, and its capacity is also the smallest size that yields the lowest LCOE for the microgrid system. The component operation hours could also explain why the hydro resource has the highest capacity in the optimal microgrid system, followed by wind, then solar. Further investigation reveals that the diesel generator operates the most during February, when the data of hydro resource production are at the lowest.

Adding renewable energy resources to KAELCO's existing energy system configuration increases renewable energy penetration from 5.29% (Scenario 1) to 39.4% (Scenario 2, Cases 2 and 3) and 45.7% (for Scenario 2, Case 1). The new energy system configurations support national programs that encourage renewable energy utilization to provide quality, reliable, and secure electricity service [66–68]. In terms of carbon emission reduction, the

new energy system configurations reduce CO_2 emissions down to 2,884,846 kg/yr (for Scenario 2, Cases 2 and 3) and 1,086,954 kg/yr (for Scenario 2, Case 1) from 25,364,376 (Scenario 1). This means that the more renewable energy sources are utilized in the energy mix, the more CO_2 emissions are reduced. Take, for example, the difference in carbon emission reduction between Scenario 2, Case 1 and Scenario 2, Case 2 and 3. Although the Philippines remains a minor contributor to global GHG emissions compared with other countries [69], increasing the percentage of renewables in the capacity mix still significantly contributes to climate change adaptation [70].

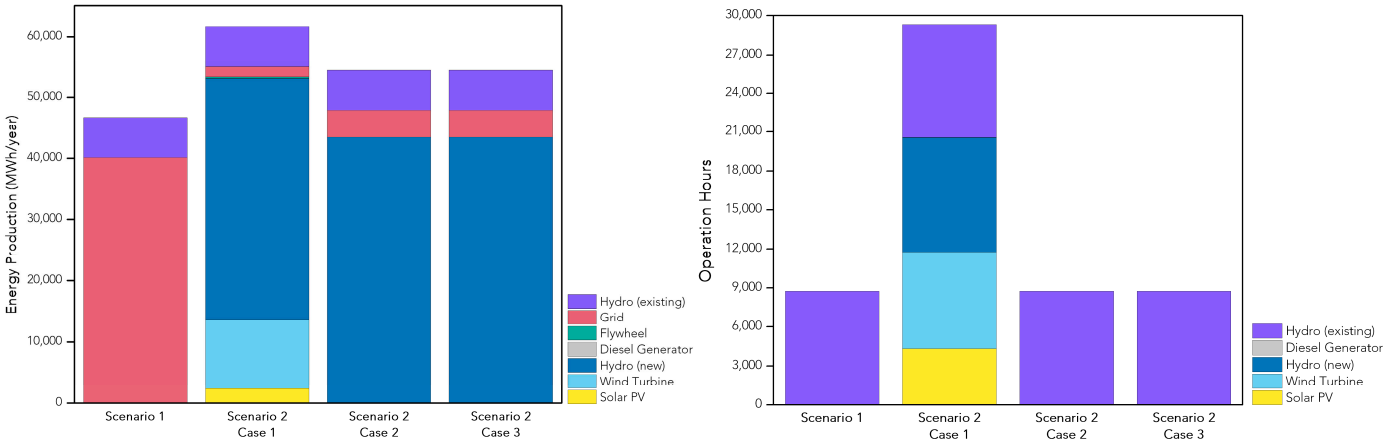

Figure 14. Energy production (**left**) and operation hours (**right**) for each component in the optimal microgrid system.

3.2.3. Sensitivity Analysis

Although the fuel cost projection from 2020 to 2050 has an average growth of 3.5% yearly [45], fuel cost increases barely affect the LCOE of a grid-connected microgrid system throughout the 20-year project lifetime, which remains lower than the base scenario. The KAELCO load demand is also estimated to increase at an average of 3.28% annually [46] throughout the project lifetime of 20 years. If KAELCO decides to meet their load demand with their existing 1 MW hydroelectric power plant and source out the rest of the demand from the grid, their current setup would be more expensive 20 years from now than adapting a grid-connected microgrid system. An increase in component costs and changes in grid reliability also do not affect grid-connected microgrid systems as much as an islanded mode system.

3.3. Network Planning

3.3.1. Power Flow Analysis

Figure 15 shows the total hourly load demand used in the power flow analysis. It also shows the total DER production in scenarios where DERs are present in the network.

To account for the integration of DERs, as well as the sellback of excess generation and energy storage, the method of determining the system loss percentage was changed accordingly. Equations (17) and (18) show how the percent system loss was calculated:

$$loss_{p.u.-noDER} = 100\% \times \frac{losses}{demand} \tag{17}$$

$$loss_{pu-no\ DER} = 100\% \times f(x)$$
$$\text{where } f(x) \begin{cases} \frac{losses}{demand}, & no\ excess \\ \frac{losses}{demand+excess}, & has\ excess \end{cases} \tag{18}$$

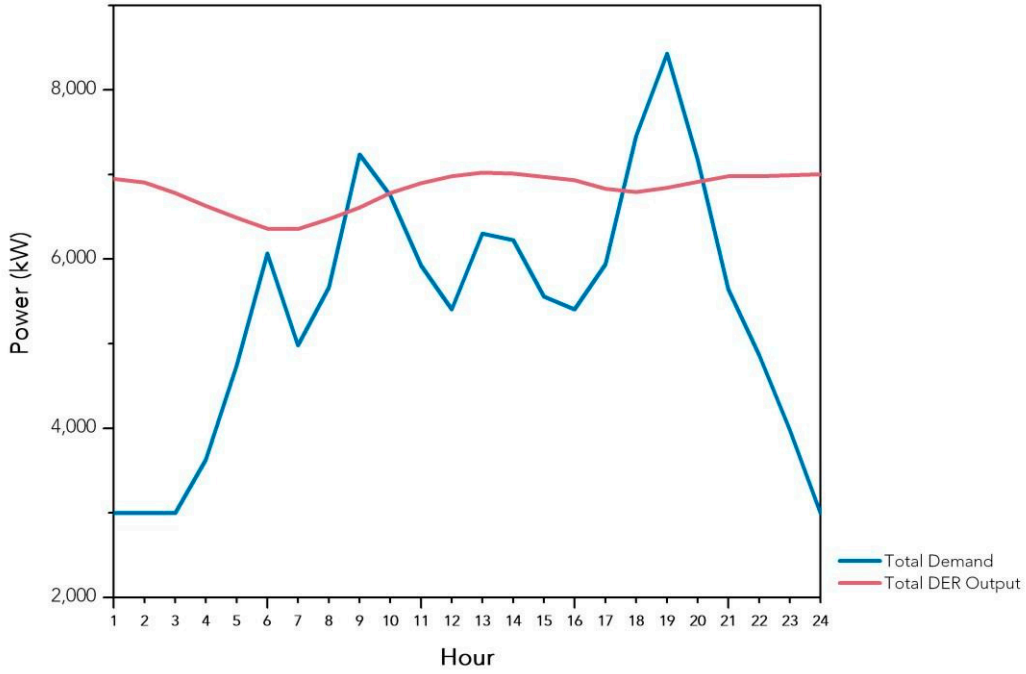

Figure 15. Comparison of total network demand and total DER production.

Figure 16 compares the hourly percent system loss experienced by the network during the before- and after-DER-integration scenarios. Here, it can be observed that, while the presence of DERs caused an increase in the overall percent system loss, the system loss in the post-DER scenario is more stable across the entire day. This is unlike the percent system loss pre-DER where an apparent maximum and minimum are seen within the day. Additionally, with the integration of the DER, the behavior of the system losses became more influenced by the total output of the DERs rather than by the total load demand.

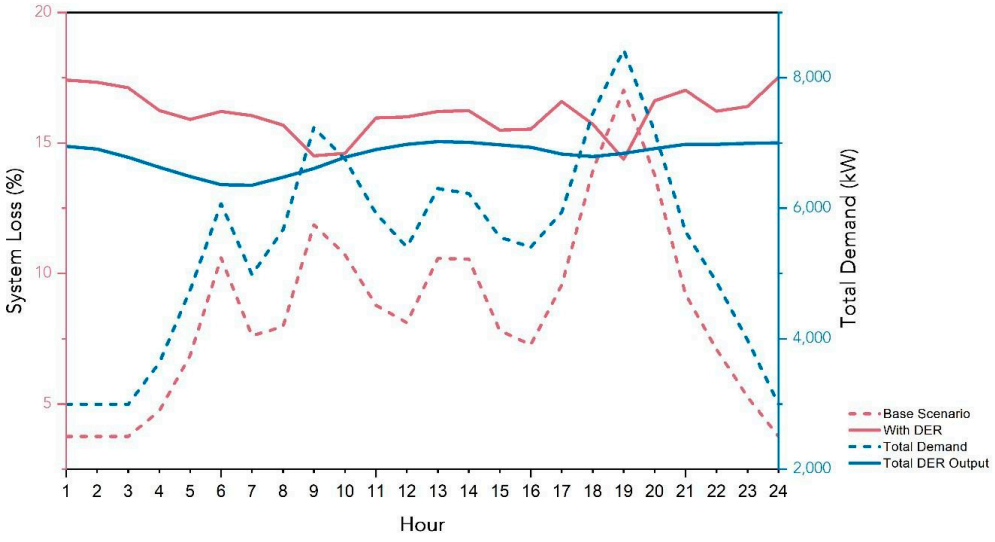

Figure 16. System losses for the base scenario and with DER overlaid on total demand and total DER output.

Figure 17 shows the distribution transformer voltages based on the load demand and the presence of DERs in the network. Feeders 1 and 2 show a significant increase in their voltages when there are DERs in the network, regardless of the load demand. Feeder 3 only shows the same increase when load demand is high. Even though the analysis treats the loads as being lumped together as large loads connected to the transformers' secondary

side, it is still possible that the loads (when disaggregated) experience a similar increase in voltage due to the presence of DERs.

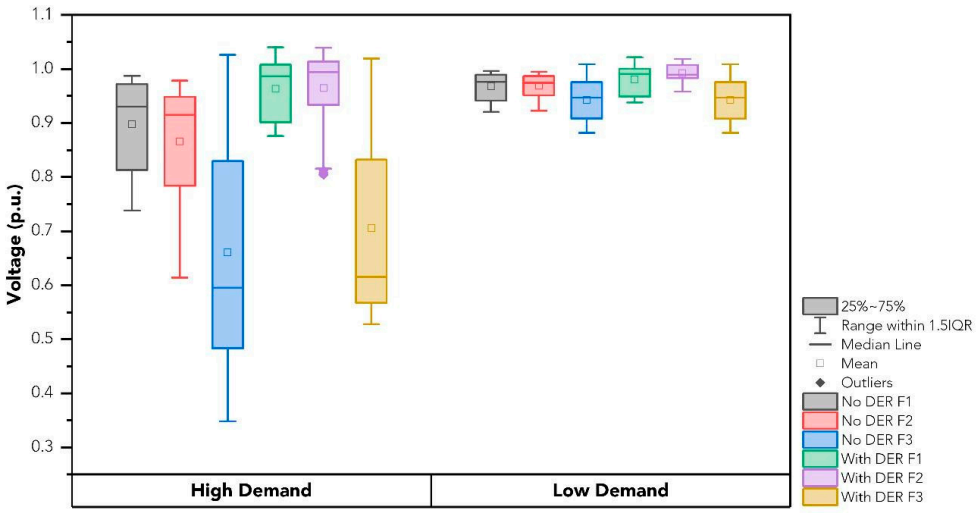

Figure 17. Comparison of transformer secondary voltages.

3.3.2. Reliability and Resiliency Analysis

The final set of potential locations for DER installation from the resource assessment is summarized in Table 11. It can be seen that six (6) locations in the franchise area of KAELCO were identified as potential sites for DERs. However, some of these locations (those with no Feeder data entries) cannot be reached by the three main feeders connected to the Tabuk Substation. Focusing only on dispatchable DERs, the final locations used in the optimal installation of new switches were the hydro resource in Upper Tabuk, Kalinga, whose feeder connection is Feeder 1. Even though diesel generation was not considered in the resource assessment, it was included in the optimal capacity mix. Hence, it was added to the list of new dispatchable DERs with its location set at the substation. Similarly, the existing hydropower plant, which is connected to Feeder 1 of the distribution network, was also considered.

Table 11. Potential locations of distributed energy resources.

Location	Solar		Hydro		Wind	
	Available	Feeder	Available	Feeder	Available	Feeder
Calanasan, Apayao	Yes	n.c.	Yes	n.c.	Yes	n.c.
Kabugao, Apayao	Yes	n.c.	-	-	Yes	n.c.
Conner, Apayao	Yes	n.c.	Yes	n.c.	-	-
Balbalan, Kalinga	Yes	3	-	-	Yes	3
Rizal, Kalinga	Yes	2	-	-	Yes	2
Pinukpuk, Kalinga	Yes	3	Yes	3	-	-
Tabuk, Kalinga	Yes	1, 3	Yes	1, 3	-	-

n.c.—not connected to feeder.

The final GRASP optimization parameters used for the optimal allocation of new switches for the network upgrade were similar to those in [30], for example, *Cswitch* = $10,000, *CEENS* = $15/kW-h, and the number of iterations = 300. The resulting optimal switch

allocation and its objective function are summarized in Table 12. These resulting switches were used in the microgrid-enabled network configuration evaluated in the reliability and resilience analysis. To determine if the improvement in the objective function is still reflected in a rural distribution utility setting, the cost of expected energy not served was reduced to *CEENS* = \$1.5/kW-h. It is apparent, as shown in Table 13, that, even at this level, microgrid investments can still improve the costs (objective function) by up to 28.98%.

Table 12. Results of the optimal switch allocation and placement based on GRASP.

Network Configuration	New Switches	Objective Function
Base scenario	none	USD 6,722,438.89
Microgrid-enabled with optimally placed switches	Feeder 1: 3 switches Feeder 2: 4 switches Feeder 3: 3 switches	USD 3,874,071.38

Table 13. Objective function of the optimal switch allocation using *CEENS* = \$1.5/kW-h.

Network Configuration	New Switches	Objective Function
Base scenario	none	USD 672,243.89
Microgrid-enabled with optimally placed switches	Feeder 1: 3 switches Feeder 2: 4 switches Feeder 3: 3 switches	USD 477,407.04

Using KAELCO's historical outage data, initial calculations were performed to obtain the failure rates and mean time to repair overhead distribution lines and distribution transformers. These values are summarized in Table 14. The number of iterations of the sequential MC was set at 1000.

Table 14. Failure rates and mean time to repair overhead distribution lines and transformers.

Component	Quantity	No. of Failures per Year	Failure Rate	Mean Time to Repair
Primary Overhead Line				
Feeder 1	26.5 km	41.50	1.566 failures/km-yr	1.07 h
Feeder 2	54.1 km	20.17	2.221 failures/km-yr	1.39 h
Feeder 3	77.5 km	45.17	0.583 failures/km-yr	1.32 h
Distribution Transformers				
Feeder 1	208	2.33	0.0112 failures/yr	0.88 h
Feeder 2	129	1.83	0.0142 failures/yr	1.26 h
Feeder 3	168	1.50	0.0089 failures/yr	1.70 h

The final reliability indices of each configuration are displayed and compared in Table 15. It can be seen that the System Average Interruption Frequency Index (SAIFI) was highly improved. This is to be expected with the addition of switches that isolate parts of the network and form islands with the DERs every time a fault occurs, lessening its impact on the network. The System Average Interruption Duration Index (SAIDI) was also reduced. With a DER in an interrupted load zone, the duration of the interruption experienced by the loads in the same load zone is lessened since power can be restored immediately after the load zone is isolated from the faulted area. The slight improvement in SAIDI may be due to the small number of dispatchable DERs installed in this extensive distribution network.

Table 15. Reliability of the microgrid-enabled network versus the base scenario network.

Network Configuration	SAIFI	SAIDI
Base scenario	197.04 customer-interruptions/year	2.3412 h/year
Microgrid-enabled	114.39 customer-interruptions/year	2.1830 h/year

The KAELCO distribution system was subjected to 100 typhoon extreme event scenarios; i.e., 100 nonsequential Monte Carlo simulations were made. A set of historical (2010–2020) daily maximum sustained wind speeds in Kalinga province was obtained from the National Aeronautics and Space Administration (NASA)'s Prediction of Worldwide Energy Resources (POWER) [71] to produce a Gumbel distribution. This probability distribution, alongside the estimated range of maximum wind speeds of typhoons [72], from the Tropical Depression category to Super Typhoon category, was used to extract the wind speed samples for every extreme event scenario. It was assumed that the area of the distribution system was small enough that the extreme typhoon event had a geographically homogenous impact. Hence, all distribution components experience the same maximum sustained wind speed level for every scenario. Moreover, due to the lack of data, the effect of the typhoon was assumed to occur instantaneously with no cascading outages after. The mean times to repair (MTTRs) of the components were obtained using the historical outage data of KAELCO. This case study assumed that the critical loads were essential to the distribution utility. Hence, the weighting factors for each priority level were 0.5 for Priority Level 4 loads, 0.3 for Priority Level 3 loads, and 0.2 for noncritical loads.

Tables 16 and 17 summarize the results of the nonsequential MC resilience assessment. It can be observed that enabling microgrid operation greatly improved the resilience of the whole system and the resilience of the loads with Priority Level 4 against typhoons, specifically, in $SAIDI_{sys}^{Typhoon}$ and $EENS_{sys}^{Typhoon}$. The addition of switches and DERs allowed faster restoration in several parts of the network; hence, customers in these parts of the network do not have to wait for the full recovery of the distribution utility after a typhoon ravaged it. The improvement in $SAIFI_{sys}^{Typhoon}$ is subtler than those in the previous two metrics. $SAIFI_{sys}^{Typhoon}$ can range from 0 (customers experience zero interruptions during typhoons) to n (all customers experience interruptions at least once during typhoons and may cascade up to n outages). From the table, regardless of the configuration, almost all customers experience an interruption during a typhoon. A probable reason for this is that pole hardening was not included in the network upgrades in the microgrid. Hence, the likelihood of poles and lines being damaged due to extreme winds remained the same despite the microgrid capability. The improvement in the level of resilience of Priority Level 4 loads shows that enabling microgrid operations is advantageous in maintaining supply to critical facilities, especially during highly disastrous situations.

Table 16. Overall resilience against typhoons of the microgrid-enabled network versus the base scenario network.

Network Configuration	$SAIFI_{sys}^{Typhoon}$	$SAIDI_{sys}^{Typhoon}$	$EENS_{sys}^{Typhoon}$
Base scenario	1.0000 customer-interruption/event	22.5362 h/event	30.1048 MWHr
Microgrid-enabled	0.9580 customer-interruption/event	13.2465 h/event	19.1168 MWHr

Table 17. Resilience against typhoons of Priority 4 Loads in the microgrid-enabled network versus Priority 4 loads in the base scenario network.

Network Configuration	$SAIFI_4^{Typhoon}$	$SAIDI_4^{Typhoon}$	$EENS_4^{Typhoon}$
Base scenario	1.0000 customer-interruption/event	22.4256 h/event	17.7762 MWHr
Microgrid-enabled	0.9558 customer-interruption/event	12.3056 h/event	10.1375 MWHr

3.3.3. Stability Analysis

Without the intervention of a microgrid-specific protection system or an islanding-enabled control system, our test case simulations show that frequency instability may occur during cases where there is a significant net power export or import from the grid. Figure 18 shows the frequency plots after islanding for various test cases. The larger the deficit or excess in the microgrid supply pre-islanding, the greater the chance of instability in the resulting microgrid during the transition period. However, there are potential solutions for improving the microgrid's stability by adding frequency-relay-based protection to drop excess generation during high pre-islanding power export.

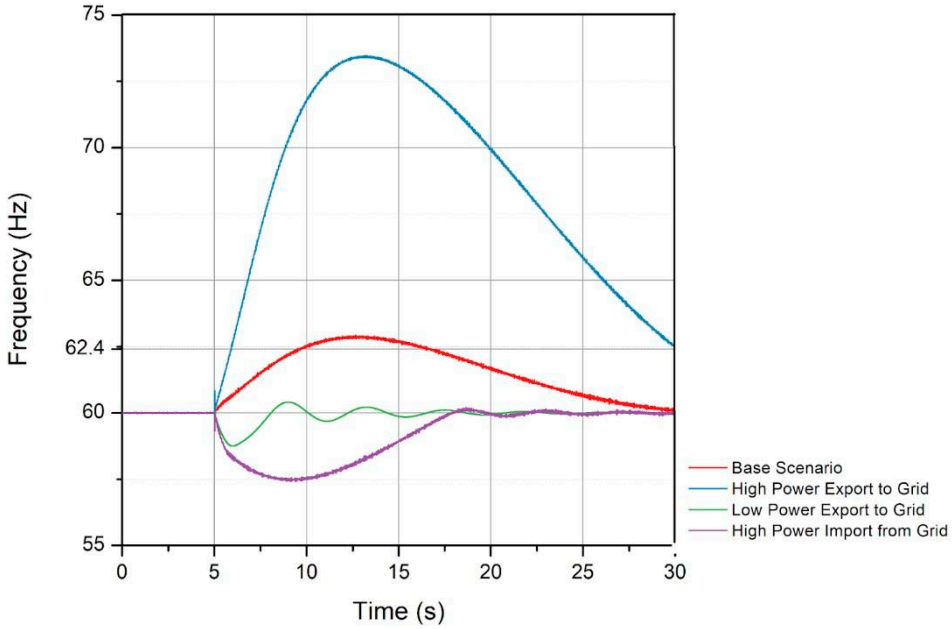

Figure 18. Frequency plots after islanding for various test cases.

It was shown that the system utilizes enough inertia in its synchronous generators to maintain a nominal frequency. The proposed diesel and hydroelectric generators allow the system to respond to the islanding event without the need for the immediate disconnection of generation. However, when the variable generation is in excess, some of the corner cases may result in over-frequency during the island transition. These will likely result in a disconnection to avoid damage. The plot in Figure 19 shows the behavior of the base scenario with frequency relays to signal breaker protection. The PV inverters are disconnected in response to the frequency relay detecting over-frequencies, and, thus, the frequency returns to a stable range due to the inertial response. A more conservative setting below the 62.4 Hz constraint shows a quicker response to allow ride-through while the synchronous generation responds to stabilize the frequency.

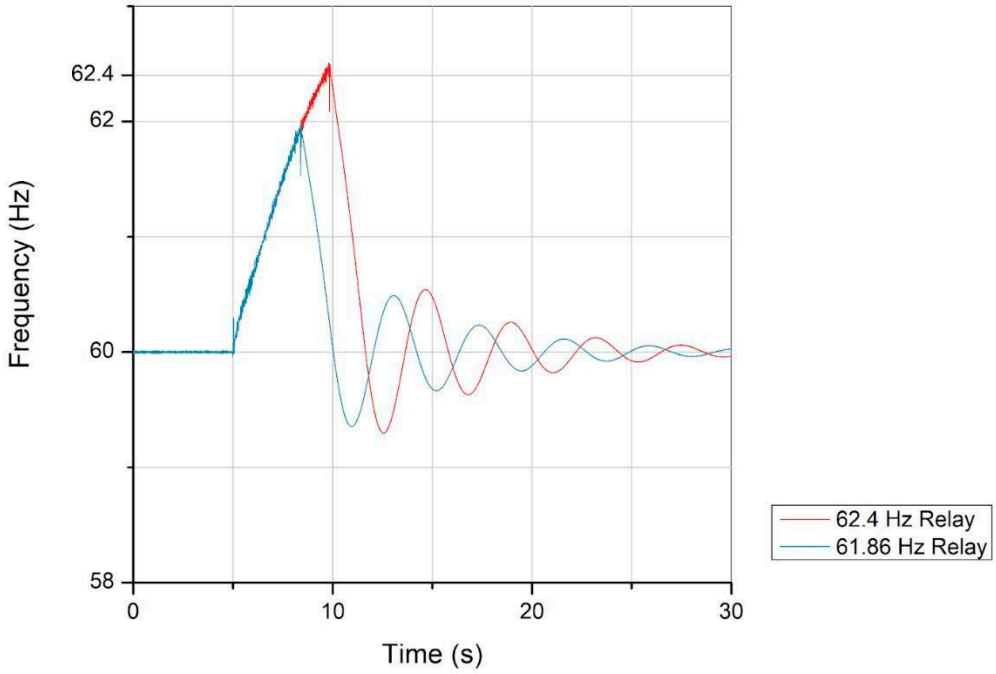

Figure 19. Frequency plots during islanding with frequency relay protection. Red and blue plots show transient behavior with the relay set at 62.4 Hz cut and 61.86 Hz, respectively.

Depending on the amount of power being imported or exported to the grid at the moment of islanding, the frequency may rise or fall beyond the regulatory constraints for safe DER operation. Using frequency relays to disconnect DER generation, such as solar or wind power, does help mitigate the resulting over-frequency, given the proper relay setting. The study recommends further exploring the conditions wherein stability may be maintained during island formation by running more experiments for a "boundary of stability" for grid power export or import and by improving the generation response by specifying the control speeds or generation inertial properties.

4. Conclusions

This work presents a utility-scale grid-connected microgrid planning framework by examining resource availability and network capability to determine the potential for microgrids, as well as, the necessary network upgrades. Results from the case study in a distribution utility in Kalinga, Philippines, show that locally available energy resources such as solar, wind, and hydro are more than enough to meet its energy demand. Adding local renewable energy resources also promotes grid flexibility and lower LCOE compared to solely relying on the main grid. And once switches and power flow were upgraded, the network could function as a microgrid seamlessly.

Results also indicate that additional switches are needed to allow the existing distribution network to operate as a network of several microgrid islands. Optimizing their locations based on load priority will help ensure that critical loads are supplied continuously. Power flow assessment also revealed the need for capacity upgrades as load growth and DERs are introduced into the network. From the perspective of reliability, enabling microgrid operations in distribution networks dramatically improves the reliability of power supply in the distribution network, both in terms of interruption frequency and duration. In terms of resilience, the duration and extent of outages resulting from resilience events, such as typhoons, can be minimized with microgrids. The DERs can supply power to a part of the total customers while some portions of the distribution network are still being repaired. Stability was shown to be good but inconsistent due to dependence on the amount of grid power export or import at the time of grid disconnection. In this case, recommendations are made for frequency relay-based protection.

The adoption of this planning framework would greatly benefit distribution utilities in maximizing the local resources and achieve sustainable energy goals that may be imposed by concerned government agencies. Though this case study focuses on Kalinga Province, the proposed planning framework is adaptable to other regions with similar energy profiles, especially in other rural areas in the Philippines as well as other developing countries. Many such regions face challenges with unreliable grids and natural disasters, making microgrids a practical solution to enhance energy access and resilience. For future studies, it is recommended to gather more information on the network characteristics of the distribution utility such as the placement and specifications of existing protection devices, switches, and reconfiguration devices across the network. Thus, the actual distribution network operation components such as system losses and reliability can be modeled with high accuracy and confidence.

Author Contributions: Conceptualization, methodology, validation, and formal analysis, G.A.A., J.A.I., P.E.D.B., L.L.F.B., X.N.P., M.T.C., E.A.E.J., K.E.P., A.E.D.T., I.B.N.C.C., J.D.O. and C.M.F.O.; writing—original draft, G.A.A., P.E.D.B., J.A.I., L.L.F.B. and X.N.P.; writing—review and editing, G.A.A., J.A.I., K.E.P., A.E.D.T., I.B.N.C.C., J.D.O. and C.M.F.O.; funding acquisition, C.M.F.O. All authors have read and agreed to the published version of the manuscript.

Funding: This work is financially supported by the Pilot Study for Integrating Microgrid and Distributed Renewable Energy Sources for an Electric Cooperative Project funded by the Department of Science and Technology [Philippines] through the Collaborative Research and Development to Leverage the Philippine Economy (CRADLE) program.

Data Availability Statement: The data and source codes presented in this study are available upon request from the corresponding author.

Acknowledgments: The authors would like to thank the DPJ Engineers and Consultants, KAELCO, and the LiPAD Team, UP Training Center for Applied Geodesy and Photogrammetry, University of the Philippines Diliman for providing the necessary data and Project CIPHER, UP Research and Development Grant, and DOST Engineering Research and Development for Technology for the APC.

Conflicts of Interest: The authors declare no conflicts of interest.

References

1. Boche, A.; Foucher, C.; Villa, L.F.L. Understanding Microgrid Sustainability: A Systemic and Comprehensive Review. *Energies* **2022**, *15*, 2906. [CrossRef]
2. Department of Energy Microgrid & PVM Database Visual Mapping. Available online: http://lookerstudio.google.com/reporting/07c4b4c5-50b5-4117-aad8-4f66d5f58458/page/p_phtf62rsyc?feature=opengraph (accessed on 5 April 2024).
3. Mahmoud, M.S. (Ed.) Chapter 1—Microgrid Control Problems and Related Issues. In *Microgrid*; Butterworth-Heinemann: Oxford, UK, 2017; pp. 1–42, ISBN 978-0-08-101753-1.
4. Kanakadhurga, D.; Prabaharan, N. Demand Side Management in Microgrid: A Critical Review of Key Issues and Recent Trends. *Renew. Sustain. Energy Rev.* **2022**, *156*, 111915. [CrossRef]
5. Järventausta, P.; Peltonen, L.; Valta, J.; Uski, S.; Aalto, P. Microgrids: Impact on the Development of Sustainable Electric Energy Systems. In *Affordable and Clean Energy*; Leal Filho, W., Marisa Azul, A., Brandli, L., Lange Salvia, A., Wall, T., Eds.; Springer International Publishing: Cham, Switzerland, 2021; pp. 905–915, ISBN 978-3-319-95864-4.
6. United Nations Environment Programme. GOAL 7: Affordable and Clean Energy. Available online: http://www.unep.org/explore-topics/sustainable-development-goals/why-do-sustainable-development-goals-matter/goal-7 (accessed on 5 April 2024).
7. Gunnarsdottir, I.; Davidsdottir, B.; Worrell, E.; Sigurgeirsdottir, S. Sustainable Energy Development: History of the Concept and Emerging Themes. *Renew. Sustain. Energy Rev.* **2021**, *141*, 110770. [CrossRef]
8. Danish, M.S.S.; Matayoshi, H.; Howlader, H.R.; Chakraborty, S.; Mandal, P.; Senjyu, T. Microgrid planning and design: Resilience to sustainability. In Proceedings of the 2019 IEEE PES GTD Grand International Conference and Exposition Asia (GTD Asia), Bangkok, Thailand, 19–23 March 2019; pp. 253–258.
9. Akinyele, D.; Belikov, J.; Levron, Y. Challenges of Microgrids in Remote Communities: A STEEP Model Application. *Energies* **2018**, *11*, 432. [CrossRef]
10. Schnitzer, D.; Lounsbury, D.S.; Carvallo, J.P.; Deshmukh, R.; Apt, J.; Kammen, D.M. *Microgrids for Rural Electrification: A Critical Review of Best Practices Based on Seven Case Studies*; United Nations Foundation: New York, NY, USA, 2014.
11. Vukojevic, A.; Lukic, S.; White, L.W. Implementing an Electric Utility Microgrid: Lessons Learned. *IEEE Electrif. Mag.* **2020**, *8*, 24–36. [CrossRef]

12. Nurunnabi, M.D.; Roy, N.K.; Pota, H.R. Optimal Sizing of Grid-Tied Hybrid Renewable Energy Systems Considering Inverter to PV Ratio—A Case Study. *J. Renew. Sustain. Energy* **2019**, *11*, 013505. [CrossRef]
13. Kizito, R.; Liu, Z.; Li, X.; Sun, K. Stochastic Optimization of Distributed Generator Location and Sizing in an Islanded Utility Microgrid during a Large-Scale Grid Disturbance. *Sustain. Energy Grids Netw.* **2021**, *27*, 100516. [CrossRef]
14. Yin, M.; Li, K.; Yu, J. A Data-Driven Approach for Microgrid Distributed Generation Planning under Uncertainties. *Appl. Energy* **2022**, *309*, 118429. [CrossRef]
15. Kamal, M.; Ashraf, I.; Fernandez, E. Energy resource planning for a rural microgrid: Comparison of results using different optimization algorithms. In Proceedings of the 2019 Second International Conference on Advanced Computational and Communication Paradigms (ICACCP), Gangtok, India, 25–28 February 2019; pp. 1–6.
16. Barik, A.K.; Das, D.C. Integrated Resource Planning in Sustainable Energy-Based Distributed Microgrids. *Sustain. Energy Technol. Assess.* **2021**, *48*, 101622. [CrossRef]
17. Khan, M.J.; Yadav, A.K.; Mathew, L. Techno Economic Feasibility Analysis of Different Combinations of PV-Wind-Diesel-Battery Hybrid System for Telecommunication Applications in Different Cities of Punjab, India. *Renew. Sustain. Energy Rev.* **2017**, *76*, 577–607. [CrossRef]
18. Manzoor, T.; Singh, P. Optimization and Techno-Economic Analysis of a Microgrid for an Industry with Intermittent Grid Service Using HOMER Software: A Case Study in Ladakh, India. *Int. J. Sci. Res. Publ.* **2021**, *11*, 460–462. [CrossRef]
19. Purlu, M.; Beyarslan, S.; Turkay, B.E. Optimal design of hybrid grid-connected microgrid with renewable energy and storage in a rural area in Turkey by using HOMER. In Proceedings of the 2021 13th International Conference on Electrical and Electronics Engineering (ELECO), Bursa, Turkey, 25–27 November 2021; pp. 263–267.
20. Boqtob, O.; El Moussaoui, H.; El Markhi, H.; Lamhamdi, T. Optimal sizing of grid connected microgrid in Morocco using Homer Pro. In Proceedings of the 2019 International Conference on Wireless Technologies, Embedded and Intelligent Systems (WITS), Fez, Morocco, 3–4 April 2019; pp. 1–6.
21. Mojtahedzadeh, S.; Najafi Ravadanegh, S.; Haghifam, M.-R. Microgrid-Based Resilient Distribution Network Planning for a New Town. *IET Renew. Power Gener.* **2021**, *15*, 3524–3538. [CrossRef]
22. Arefifar, S.A.; Mohamed, Y.A.-R.I. DG Mix, Reactive Sources and Energy Storage Units for Optimizing Microgrid Reliability and Supply Security. *IEEE Trans. Smart Grid* **2014**, *5*, 1835–1844. [CrossRef]
23. Mokhtari, M.B.; Vazinram, F.; Gandomkar, M. Dynamic and Stability Analysis of Microgrids with Synchronous Machines in Grid-Connected and Islanded Modes. In Proceedings of the 2012 16th IEEE Mediterranean Electrotechnical Conference, Hammamet, Tunisia, 25–28 March 2012; pp. 788–791.
24. Majumder, R. Some Aspects of Stability in Microgrids. *IEEE Trans. Power Syst.* **2013**, *28*, 3243–3252. [CrossRef]
25. QGIS Development Team. QGIS. Available online: https://qgis.org/download/ (accessed on 10 February 2021).
26. Hofierka, J.; Súri, M.; Marecka, M. The solar radiation model for Open source GIS: Implementation and applications. In Proceedings of the Open Source GIS-GRASS Users Conference, Trento, Italy, 11–13 September 2002.
27. Duffie, J.A.; Beckman, W.A. Available Solar Radiation. In *Solar Engineering of Thermal Processes*; John Wiley & Sons, Ltd.: Hoboken, NJ, USA, 2013; pp. 43–137, ISBN 978-1-118-67160-3.
28. NOAA US Department of Commerce. Solar Calculation Details. Available online: https://gml.noaa.gov/grad/solcalc/calcdetails.html (accessed on 5 April 2024).
29. Department of Energy Philippines. List of Identified Ancestral Domain (ADs) per Region. Available online: https://www.doe.gov.ph/eicc/list-identified-ancestral-domain-ads-region (accessed on 5 April 2024).
30. Hansen, M.C.; Potapov, P.V.; Moore, R.; Hancher, M.; Turubanova, S.A.; Tyukavina, A.; Thau, D.; Stehman, S.V.; Goetz, S.J.; Loveland, T.R.; et al. High-Resolution Global Maps of 21st-Century Forest Cover Change. Available online: https://glad.earthengine.app/view/global-forest-change (accessed on 5 April 2024).
31. Department of Public Works and Highways ATLAS. 2022. Available online: https://dpwh.gov.ph/dpwh/DPWH_ATLAS/06%20Road%20WriteUp%202021.pdf (accessed on 6 April 2024).
32. Elliott, D. *Philippines Wind Energy Resource Atlas Development*; National Renewable Energy Laboratory: Kuala Lumpur, Malaysia, 2000.
33. Bañuelos-Ruedas, F.; Angeles-Camacho, C.; Rios-Marcuello, S.; Bañuelos-Ruedas, F.; Angeles-Camacho, C.; Rios-Marcuello, S. Methodologies Used in the Extrapolation of Wind Speed Data at Different Heights and Its Impact in the Wind Energy Resource Assessment in a Region. In *Wind Farm—Technical Regulations, Potential Estimation and Siting Assessment*; IntechOpen: London, UK, 2011; ISBN 978-953-307-483-2.
34. Homer Pro Weibull Distribution. Available online: https://homerenergy.com/products/pro/docs/3.15/weibull_distribution.html (accessed on 6 April 2024).
35. Meyers, J.; Meneveau, C. Optimal Turbine Spacing in Fully Developed Wind Farm Boundary Layers. *Wind Energy* **2012**, *15*, 305–317. [CrossRef]
36. Kostić, S.; Stojković, M.; Prohaska, S.; Vasović, N. Modeling of River Flow Rate as a Function of Rainfall and Temperature Using Response Surface Methodology Based on Historical Time Series. *J. Hydroinform.* **2016**, *18*, 651–665. [CrossRef]
37. Ocon, J.D.; Bertheau, P. Energy Transition from Diesel-Based to Solar Photovoltaics-Battery-Diesel Hybrid System-Based Island Grids in the Philippines—Techno-Economic Potential and Policy Implication on Missionary Electrification. *J. Sustain. Dev. Energy Water Environ.* **2019**, *7*, 139–154. [CrossRef]

38. Lee, N.; Dyreson, A.; Hurlbut, D.; McCan, M.I.; Neri, E.; Reyes, N.C.; Capongcol, M.; Cubangbang, H.; Agustin, B.; Bagsik, J.; et al. *Ready for Renewables: Grid Planning and Competitive Renewable Energy Zones (CREZ) in the Philippines*; U.S. Department of Energy: Washington, DC, USA, 2020; p. NREL/TP-7A40-76235.
39. Pascasio, J.D.A.; Esparcia, E.A.; Castro, M.T.; Ocon, J.D. Comparative Assessment of Solar Photovoltaic-Wind Hybrid Energy Systems: A Case for Philippine off-Grid Islands. *Renew. Energy* **2021**, *179*, 1589–1607. [CrossRef]
40. Amber Kinetics Amber Kinetics M32 Data Sheet. Available online: https://www.amberkinetics.com/wp-content/uploads/2020/05/Amber-Kinetics-DataSheet.pdf (accessed on 21 August 2021).
41. Homer Pro Levelized Cost of Energy. Available online: https://homerenergy.com/products/pro/docs/3.15/levelized_cost_of_energy.html (accessed on 6 April 2024).
42. Homer Pro Multi-Year Inputs. Available online: https://homerenergy.com/products/pro/docs/3.15/multiyear_inputs.html (accessed on 6 April 2024).
43. Energy Regulatory Commission 2020 Annual Report. 2020. Available online: https://www.erc.gov.ph/Advisories (accessed on 13 September 2021).
44. Jordan, D.C.; Kurtz, S.R. Photovoltaic Degradation Rates—An Analytical Review. *Prog. Photovolt. Res. Appl.* **2013**, *21*, 12–29. [CrossRef]
45. U.S. Energy Information Administration. *Cost and Performance Characteristics of New Generating Technologies*; U.S. Energy Information Administration: Washington, DC, USA, 2023.
46. Kalinga Apayao Electric Cooperative, Inc. *Power Supply Procurement Plan 2021*; Kalinga Apayao Electric Cooperative, Inc.: Kalinga, Philippines, 2021.
47. Energy Regulatory Commission. *A Resolution Adopting the ERC Rules for Setting the Distribution System Loss Cap and Establishing Performance Incentive Scheme for Distribution Efficiency*; Energy Regulatory Commission: Metro Manila, Philippines, 2017.
48. Dugan, R.C.; Montenegro, D. *The Open Distribution System Simulator (OpenDSS)*; Electric Power Research Institute: Palo Alto, CA, USA, 2021.
49. Gautam, P.; Piya, P.; Karki, R. Resilience Assessment of Distribution Systems Integrated With Distributed Energy Resources. *IEEE Trans. Sustain. Energy* **2021**, *12*, 338–348. [CrossRef]
50. Ghosh, D. Resilience Assessment of Microgrid Using Complex Network Theory. In Proceedings of the 2021 1st International Conference on Power Electronics and Energy (ICPEE), Bhubaneswar, India, 2–3 January 2021; pp. 1–6.
51. Abantao, G.A.; Ibañez, J.A.; Bundoc, P.E.D.C.; Blas, L.L.F.; Penisa, X.N.; Esparcia, E.A.; Castro, M.T.; Buendia, R.V.E.; Pilario, K.E.S.; Tio, A.E.D.; et al. Reconceptualizing Reliability Indices as Metrics to Quantify Power Distribution System Resilience. *Energies* **2024**, *17*, 1909. [CrossRef]
52. López, J.C.; Franco, J.F.; Rider, M.J. Optimisation-Based Switch Allocation to Improve Energy Losses and Service Restoration in Radial Electrical Distribution Systems. *IET Gener. Transm. Distrib.* **2016**, *10*, 2792–2801. [CrossRef]
53. Kundur, P. *Power System Stability and Control*; McGraw-Hill: New York, NY, USA, 1994.
54. Abantao, G.A.; Ibanez, J.A.; Bundoc, P.E.D.C.; Blas, L.L.; Penisa, X.N.; Pilario, K.E.S.; Tio, A.E.D.C.; Cruz, I.B.N.C.; Ocon, J.D.; Odulio, C.M.F. Generation and Network Planning of Utility-Scale Grid-Connected Microgrids. *Chem. Eng. Trans.* **2023**, *103*, 877–882. [CrossRef]
55. Energy Regulatory Commission. *Philippine Grid Code*; Energy Regulatory Commission: Metro Manila, Philippines, 2001.
56. Kalinga Apayao Electric Cooperative, Inc. *Power Supply Procurement Plan 2019*; Kalinga Apayao Electric Cooperative, Inc.: Kalinga, Philippines, 2019.
57. Congress of the Philippines. *Republic Act No. 7586*; Congress of the Philippines: Quezon, Philippines, 1992.
58. Congress of the Philippines. *Republic Act No. 8371*; Congress of the Philippines: Quezon, Philippines, 1997.
59. Bautista, M.L.P.; Bautista, B.; Narag, I.C.; Aquino, A.D.; Papiona, K.; Delos Santos, A.L.; Nadua, J.; Deximo, J.P.; Sevilla, W.I.; Melosantos, L.P.; et al. *Enhancing Risk Analysis Capacities for Flood, Tropical Cyclone Severe Wind and Earthquake for Greater Metro Manila Area—Summary Report—Philippines | ReliefWeb*; Republic of the Philippines and the Commonwealth of Australia (Geoscience Australia): Symonston, Australia, 2014.
60. Thornburg, D.W.; Kimball, C.; Bracken, W.C. *2018 International Building Code Illustrated Handbook*, 1st ed.; McGraw-Hill Education: New York, NY, USA, 2018; ISBN 978-1-260-13229-8.
61. DOST-UP DREAM and Phil-LiDAR Program LiPAD—LiDAR Portal for Archiving and Distribution. Available online: https://lipad.dream.upd.edu.ph/ (accessed on 6 April 2024).
62. Chaves, A.; Bahill, A.T. *ArcUser*; Esri: Redlands, CA, USA, 2010; pp. 24–27.
63. Power Sector Assets and Liabilities Management Corporation (PSALM). *ERC Case No. 2013-169 RC*; Power Sector Assets and Liabilities Management Corporation (PSALM): Quezon, Philippines, 2013.
64. Homer Pro Load Following Strategy. Available online: https://homerenergy.com/products/pro/docs/3.15/load_following_strategy.html (accessed on 6 April 2024).
65. Ahmed, S.J. *Philippines Power Sector Can Reach Resilience by 2021*; Institute for Energy Economics and Financial Analysis: Lakewood, OH, USA, 2020; p. 1.
66. Department of Energy. *Promulgating the Rules and Guidelines Governing the Establishment of the Renewable Portfolio Standards for On-Grid Areas*; Department of Energy: Taguig, Philippines, 2017.

67. Department of Energy. *Promulgating the Rules and Guidelines Governing the Establishment of the Green Energy Option Program Pursuant to the Renewable Energy Act of 2008*; Department of Energy: Taguig, Philippines, 2018.
68. Congress of the Philippines. *Republic Act No. 11646*; Congress of the Philippines: Quezon, Philippines, 2022.
69. Phoumin, H.; Kimura, S.; Abdurrahman, S.; Sirikum, J.; Manaligod, L.R.A.; Zulkifli, Z. *Distributed Energy System in Southeast Asia*; Economic Research Institute for ASEAN and East Asia: Jakarta, Indonesia, 2018; pp. 106–138.
70. International Renewable Energy Agency (IRENA). *Bracing for Climate Impact: Renewables as a Climate Change Adaptation Strategy*; International Renewable Energy Agency (IRENA): Abu Dhabi, United Arab Emirates, 2021.
71. National Aeronautics and Space Administration. Prediction Of Worldwide Energy Resources (POWER). Available online: https://power.larc.nasa.gov/data-access-viewer/ (accessed on 25 August 2021).
72. Philippine Atmospheric, Geophysical and Astronomical Services Administration (PAGASA) About Tropical Cyclones. Available online: https://www.pagasa.dost.gov.ph/information/about-tropical-cyclone (accessed on 7 April 2024).